

<https://doi.org/10.1038/s43246-024-00612-2>

# Recent advances in drug delivery systems for osteosarcoma therapy and bone regeneration

Check for updates

Sally Kortam , Zufu Lu &amp; Hala Zreiqat

Osteosarcoma, the predominant bone malignancy, poses significant challenges due to its high metastatic potential and recurrence rates. Accounting for a substantial percentage of malignant bone tumors, osteosarcoma particularly affects children and adolescents. Despite standard treatment combining surgery and multi-drug chemotherapy, systemic drug administration presents limitations, leading to compromised patient quality of life and severe side effects. New strategies are needed to address these challenges and enhance efficacy while minimizing toxicity. Here, we explore drug delivery platforms in the context of osteosarcoma treatment. We delve into both systemic and local delivery approaches, highlighting recent advances in controlled drug release triggered by various stimuli, modifications for targeted delivery, and co-delivery of chemotherapeutics using nano-platforms. Additionally, we discuss innovations in local delivery methods, including implantable nanoparticles, injectable hydrogels, and scaffolds. Despite these advancements, challenges and limitations persist, emphasizing the need for continued research. We conclude by offering perspectives on the potential of multifunctional scaffolds in revolutionizing osteosarcoma drug delivery, thereby paving the way for improved patient survival and enhanced quality of life.

Osteosarcoma (OS), the most common bone malignancy, arises from bone and cartilage and accounts for approximately 55% of all primary malignant bone tumors<sup>1</sup>. OS is the third most common malignancy among children and adolescents between the ages of 12 and 18<sup>2</sup>, following leukemia and lymphoma, with a yearly incidence of 5.6 cases per million in children under the age of 15<sup>3</sup>. OS is notorious for its high rates of metastasis and recurrence, with 15% to 20% of patients presenting clinically detectable metastases at diagnosis. The lungs, the primary site of metastasis, account for over 85%, while bone represents the second most common distant disease site<sup>4</sup>. Recurrent OS affects 30-50% of those with initial localized disease and 80% of patients with metastatic conditions, with the lungs being the predominant site of recurrence<sup>5</sup>.

Standard OS treatment involves a combination of surgery and multi-drug chemotherapy. Surgical intervention aims to excise the tumor with optimal margins while preserving functionality. Pre- and post-operative chemotherapy, consisting of doxorubicin (DOX), methotrexate (MTX), and cisplatin (CDDP), aims to shrink the tumor pre-resection and eliminate residual tumor post-resection<sup>6</sup>. However, systemic chemotherapy presents challenges such as invasiveness and pain, significantly compromising patients' quality of life. Systemic drug administration faces limitations in

reaching neoplastic cells distant from tumor vessels, leading to suboptimal drug concentration in cancerous bone tissue. This arises from factors like drug instability in blood, protein binding, and liver Kupffer cell clearance, resulting in dose-related toxicity<sup>7</sup>. Consequently, high systemic doses are often necessary, causing severe side effects such as myelosuppression, hepatotoxicity, cardiotoxicity, and fatal central nervous system disturbances<sup>8</sup>. More than 30% of OS patients are either resistant to current chemotherapy or experience life-threatening complications, ultimately leading to the progression of metastases and mortality<sup>9</sup>.

To address these challenges, it is crucial to develop novel strategies with reduced toxicity and enhanced efficacy to improve patient survival and quality of life. Recently, nanoparticle-based drug delivery platforms have been introduced to deliver anti-cancer agents for OS. These nanoparticle systems have shown several advantages over traditional systemic chemotherapy for treating OS, including reduced adverse effects, improved drug pharmacokinetics, and extended circulation time in the bloodstream. Despite these significant advantages, this approach suffers from notable limitations, primarily that only a small fraction of systemically administered drugs, often less than 5%, reach the targeted tumor site. Consequently, recent efforts have shifted towards local drug delivery using multiple

Biomaterials and Tissue Engineering Research Unit, School of Biomedical Engineering, The University of Sydney, Sydney, NSW, 2006, Australia.

 e-mail: [hala.zreiqat@sydney.edu.au](mailto:hala.zreiqat@sydney.edu.au)

approaches. The local delivery strategy bypasses the limitations encountered by nanoparticles (NPs) in the bloodstream before reaching the target site, especially in bone tissue, and offers greater potential for the effective release of anti-cancer drugs to treat OS.

In this comprehensive review, we delve into common NPs used as drug carriers in OS, highlighting recent advances in controlled drug release strategies triggered by various stimuli, modifications for targeted drug delivery, and co-delivery of chemotherapeutics using nano-platforms. Additionally, we explore advancements in local delivery, encompassing implantable NPs, injectable hydrogels, and scaffolds (Fig. 1). The review concludes by outlining the challenges and limitations of multifunctional scaffolds in OS drug delivery, including the impact of therapeutic agents on healthy cells, the limitations of current tumor models, and the need for more relevant preclinical animal models.

## Systemic NPs-based drug delivery

Within the past few decades, the field of nanotechnology and nanomedicine has remarkably developed and actively been applied to various diseases such as cancer, infection, skin-related diseases, cardiovascular-related diseases, and regeneration like bone, teeth, and wound healing<sup>10</sup>. The majority of research publications in the field of nanomedicine focus on the use of NPs in drug delivery, mainly as drug carriers to deliver proteins, growth factors, and other chemical drugs. NPs are broadly classified into various categories depending on their physical properties (e.g., morphology and size) and chemical characteristics. Nevertheless, they can be divided into four main categories: polymeric NPs (made of polymers like poly (lactic-coglycolic acid), dextran, and chitosan), metal NPs (e.g., gold, silver, and copper), ceramic NPs (e.g., calcium phosphates and mesoporous silica) and lipid-based NPs (mainly liposomes) (Fig. 2).

There are four primary routes for administering NPs: injection, inhalation, oral intake, and intravenous administration, with the latter being predominantly used in *in vivo* studies related to OS research<sup>11–14</sup>. The Synthesis of NPs generally follows top-down or bottom-up protocols. Top-down methods involve breaking down larger materials into nanoparticles suitable for drug delivery, while bottom-up techniques entail the assembly of smaller building blocks to form larger particles<sup>15</sup>.

### NPs categories

**Polymeric NPs.** Polymeric NPs range in size from 1 to 1000 nm and can be derived from either natural or synthetic polymers. Examples of natural polymers include chitosan, dextran, and gelatin, whereas synthetic polymers encompass materials like poly( $\epsilon$ -caprolactone) (PCL), poly (ethylene glycol) (PEG), and poly(lactide-co-glycolide) (PLGA)<sup>16,17</sup>,

Natural polymeric NPs. The primary advantages of natural polymeric NPs lie in their availability in nature, biodegradability, biocompatibility, and low toxicity. However, they may pose immunogenicity concerns and often necessitate chemical modification prior to their utilization in NPs development<sup>15</sup>.

Keratin, a natural polymer, has unique tri-peptidic sequences such as “Arg–Gly–Asp” (RGD) and “Leu–Asp–Val” (LDV) sequences that bind to vitronectin integrin receptors, which are overexpressed by OS cells. Keratin was functionalized with the photosensitizer Chlorin-e6 and then loaded with the chemotherapeutic drug Paclitaxel (PTX) to create PTX-keratin NPs<sup>18</sup>. *In vitro* toxicity tests on OS cell lines in 2D and 3D systems showed that PTX and Ce6 have an additive effect. The combined cytostatic blockage of PTX and oxidative damage from reactive oxygen species (ROS) upon light irradiation had a superior effect compared to PTX or Ce6 alone. MTX is a widely used chemotherapy for the treatment of various cancers. Despite its efficacy in fighting cancer, MTX's severe toxicity towards normal cells and low water solubility present limitations in its clinical use. To address these challenges, Li et al.<sup>19</sup> developed poloxamer-modified trimethyl chitosan-encapsulated MTX. The resulting NPs showed increased cytotoxicity in human OS MG-63 cells *in vitro* when compared to free MTX due to improved cellular uptake.

Synthetic polymeric NPs. While natural polymeric NPs offer superior biocompatibility and lower toxicity compared to their synthetic polymeric NPs, synthetic polymeric NPs have garnered attention due to their stability and flexibility in obtaining polymeric materials. Moreover, the ability to synthesize these materials tailored to specific pathologies and patient needs underscores the advantages of synthetic polymeric NPs over natural ones<sup>20</sup>.

NPs made of synthetic PLGA polymer are widely applied in drug delivery because of their biodegradable and biocompatible features. Irmak et al.<sup>21</sup> encapsulated Salinomycin, an antibacterial and therapeutic agent known for its suppressive effects on the proliferation of different cancer stem cells, including OS, within PLGA NPs to address Salinomycin's poor aqueous solubility. *In vitro* experiments utilizing an apoptosis assay revealed that PLGA NPs loaded with Salinomycin induced heightened apoptosis in OS MG-63 cells compared to unencapsulated Salinomycin, attributed to increased caspase-3 expression and decreased levels of c-myc and  $\beta$ -catenin.

In addition to drug delivery, PLGA and other polymers, such as PEG, are commonly utilized to modify nanocarriers to enhance stability, biocompatibility, and circulation time in the body<sup>22–24</sup>. Notably, these polymers have been instrumental in addressing the challenge of initial burst release in NPs. For instance, Ray et al.<sup>25</sup> developed LDH-MTX NPs by incorporating MTX with a Mg-Al- layered double hydroxide nanoceramic matrix. To prevent the initial burst release of MTX, they encapsulated the NPs in PLGA polymer. Results indicated that PLGA-LDH-MTX and PLGA-MTX NPs were both effective in suppressing tumor growth in subcutaneous mouse model compared to free MTX. PLGA-LDH-MTX was even more effective in terms of antitumor activity than bare MTX and PLGA-MTX, with a reduced likelihood of side effects when the same dose of MTX drug content was applied.

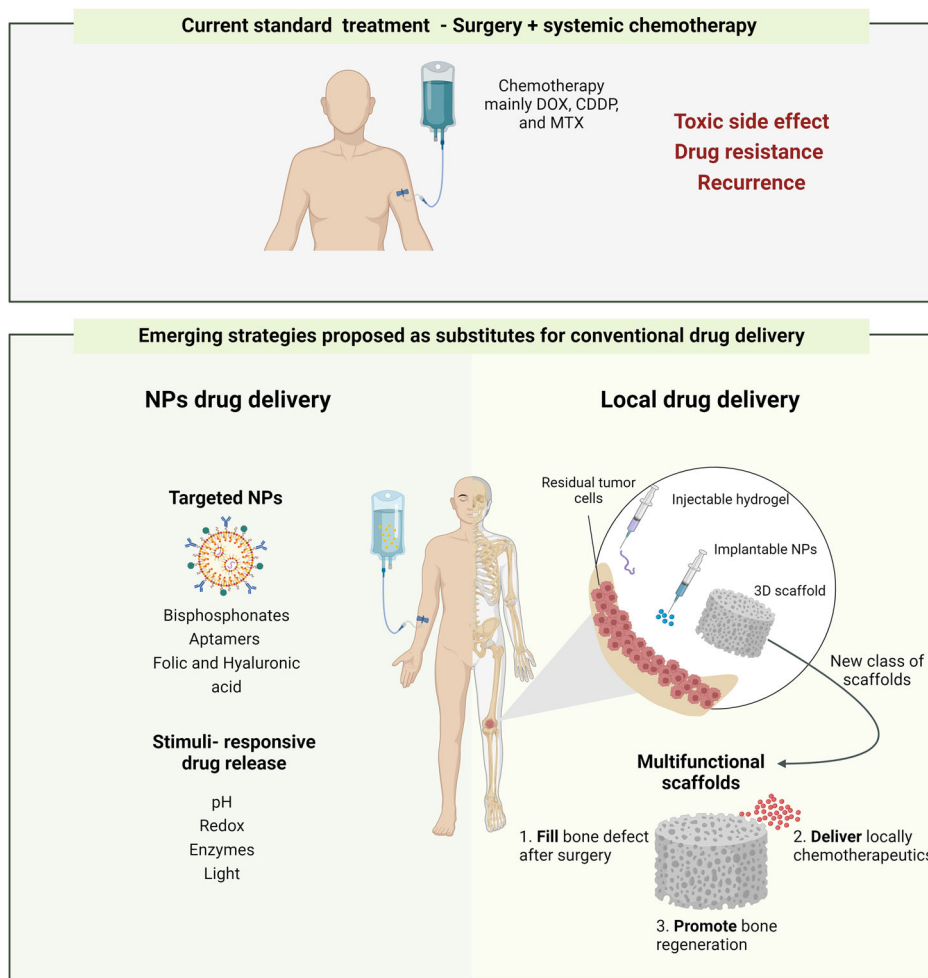
**Metal NPs.** In recent years, metal NPs, derived from bulk metals, have been extensively utilized in diagnostic imaging and drug delivery applications due to their physical and chemical properties, including mechanical strength, high surface area, thermal, optical, catalytic, and magnetic properties<sup>26</sup>. Metal NPs can be classified into two main categories. The first category is NPs that are composed of pure metals, e.g., silver, copper, gold, titanium (Ti), platinum, zinc, magnesium (Mg), iron, and alginate NPs. The second category is metal oxide NPs such as iron oxide (magnetic NPs), Ti dioxide, silver oxide, zinc oxide, etc.<sup>27</sup>.

Most metal oxide NPs have intrinsic anticancer properties, eliminating the need to load them with chemotherapy drugs<sup>28–31</sup>. Pure metal NPs, especially gold NPs, are primarily used in photothermal therapy<sup>32,33</sup>. Additionally, metals have been reported as drug carriers in the treatment of OS. For instance, Popescu et al.<sup>34</sup> utilized magnetite Fe<sub>3</sub>O<sub>4</sub> NPs as carriers for Gemcitabine to enhance the cytotoxic effects of this chemotherapeutic agent on cancer cells, including OS MG-63 cell lines.

Superparamagnetic iron oxide NPs (SPIONs) are gaining widespread attention due to their biocompatibility and sensitivity to an applied magnetic field, yet unmodified simple SPIONs are prone to aggregation and unstable in biological conditions. Puiu et al.<sup>35</sup> applied  $\beta$ -Cyclodextrin as a surface modifier for SPIONs to make them water-dispersible and to enable the loading of the hydrophobic anti-cancer drug PTX. The results from MTT assays showed that  $\beta$ -CD surface-modified SPIONs exhibited excellent biocompatibility, demonstrating no cytotoxic effects toward MC3T3-E1 murine osteoblasts. Meanwhile, the PTX-loaded  $\beta$ -CD surface-modified SPIONs significantly reduced the cell viability of the OS MG-63 cell line by 85%.

**Ceramic NPs.** Ceramic NPs are primarily comprised of carbides, oxides, carbonates, and phosphates of metals and metalloids. Examples of commonly used ceramic NPs include silica, alumina, titania, zirconia, calcium phosphates, calcium carbonate and hydroxyapatite (HAp). In recent years, remarkable progress has been made in the research on ceramic NPs for biomedical applications, especially in orthopedic and dental treatments, thanks to their unique processing, high mechanical strength, toughness and bioactivity<sup>36–39</sup>.

**Fig. 1 | Standard and emerging osteosarcoma treatment strategies.** An illustration of current standard treatment for osteosarcoma alongside new alternative drug delivery methods, providing an outline of the review article's structure. Created with BioRender.com.



Among various ceramic NPs, HAp NPs have been extensively studied in OS research due to their structural similarity to bone apatite, which enhances their biocompatibility and noninflammatory properties<sup>36,40–44</sup>. In their study, Zhou and his team<sup>41</sup> developed Selenium-doped HAp nanowire/chitosan (Se-HAp/CSP) biopapers. When co-cultured with both cancerous and normal cells, the Se-HAp/CSP composite biopapers exhibited increased toxicity towards tumor cell lines compared to normal bone marrow stromal cells. Furthermore, anti-tumor experiments using a patient-derived xenograft tumor mouse model confirmed the ability of the Se-HAp/CSP biopapers to suppress tumor growth.

Calcium carbonate is another ceramic that is used in OS research<sup>12,38,45,46</sup>. Li et al.<sup>12</sup> developed organic-inorganic hybrid NPs based on calcium carbonate mineralization of polymers. These NPs offer several benefits, including pH sensitivity, small size, high biocompatibility, and biodegradability. Known as DOX-loaded calcium carbonate-crosslinked polypeptide NPs, they exhibited high drug loading capacity, improved cellular uptake, and increased cytotoxicity against mouse OS cells. Furthermore, they demonstrated enhanced antitumor efficacy and reduced side effects in subcutaneous and orthotopic OS mouse models.

The potential of ceramic NPs in sustained drug delivery has been hindered by their limited drug loading capacity, initial burst release, and short-term release. To overcome these challenges, researchers have explored the use of a combination of ceramic NPs with polymers as a strategy to enhance drug release and mechanical properties. Dan Son et al.<sup>47</sup> investigated the use of calcium phosphate NPs containing anticancer drug in the presence of alginate as means to stabilize the nanocomposites. The resulting nanocomposites exhibited an initial burst release of the drug, followed by a slow and long-term release rate. Furthermore, the release profile was found to be dependent on the pH of the solution, with faster drug release observed

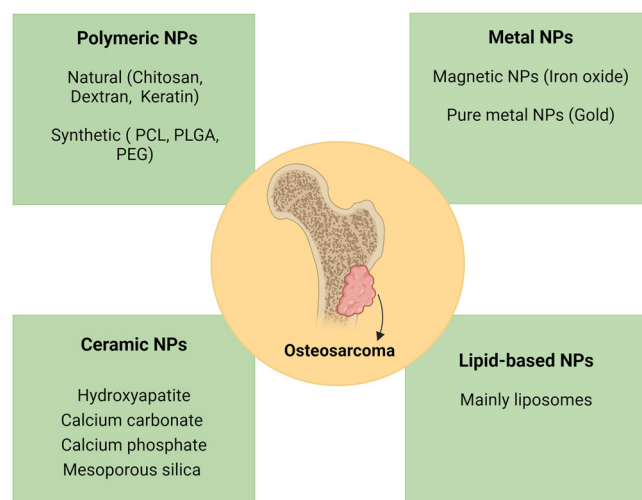


**Fig. 2 | Different types of nanoparticles used for osteosarcoma.** NPs used in osteosarcoma research are primarily categorized into four groups: polymeric NPs, metal NPs, ceramic NPs, and lipid-based NPs (mainly liposomes). Created with BioRender.com.

at pH 4.5 compared to pH 7.4. Ghosh et al.<sup>42</sup> synthesized a novel nanocomposite by coating HAp NPs with DOX and further modifying them with chitosan. The purpose of this modification was to enhance the mechanical and biological properties of the nanocomposite. The results of their study

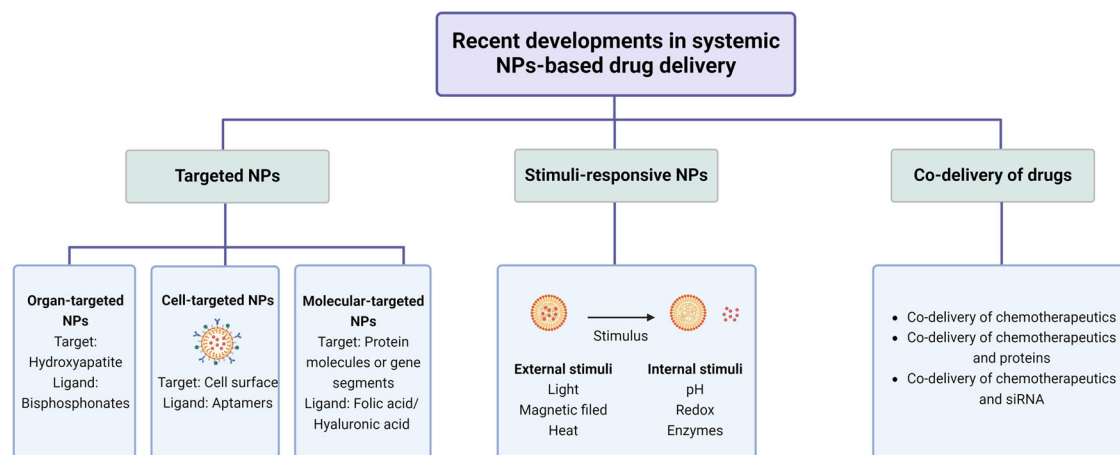


**Fig. 3 | Recent developments in systemic NPs-based drug delivery.** Recent advancements in NPs-based drug delivery include targeted drug delivery, stimulus-responsive drug delivery, and co-delivery of multiple drugs. Created with BioRender.com.

showed that the HAP NPs alone were biocompatible with OS MG-63 cells, whereas the developed nanocomposite exhibited cytotoxicity towards OS MG-63 cells.

**Liposomes NPs.** Liposomes, the first FDA-approved therapeutic NPs, range in size from nanosized to micronized (20 nm up to several micrometers) and are closed vesicles with a bilayer structure. They are naturally produced by dispersing amphipathic molecules, such as phospholipids, in an aqueous environment. Liposomes have been extensively used as carriers of various drugs, including chemotherapeutics and antibiotics, thanks to their various advantages; these include the capability of holding both hydrophilic and lipophilic drugs, biocompatibility, low-immunogenicity, non-toxicity, and high drug encapsulation efficiency.

Additionally, the modification of liposomal surfaces is straightforward, and several strategies for their surface modification have been established, including polymer coating, altering surface charge, and modification with ligands<sup>48,49</sup>.

The unique structure of liposomes, featuring a hydrophilic core surrounded by a phospholipid bilayer, allows the encapsulation of both lipophilic and hydrophilic drugs. Lipophilic drugs are integrated into the lipid bilayer, while hydrophilic drugs are entrapped in the inner space of the liposomal carrier, making liposomes ideally suited for the co-delivery of multiple drugs with different pharmacokinetic properties<sup>50</sup>.

To enhance stability and prolong circulation half-time, liposomes can be coated with biocompatible hydrophilic polymers, most notably PEG, resulting in PEGylated liposomes. The PEG coating facilitates the escape of liposomes from the reticuloendothelial system (RES), thereby extending their circulation time in the bloodstream. Additionally, PEG reduces particle aggregation through steric hindrance stabilization, ultimately enhancing the stability of liposomes<sup>51</sup>. Haghirsadat et al.<sup>52,53</sup> demonstrated an approach to augment the cellular uptake of DOX in various OS cell lines by developing a PEGylated DOX-loaded liposomal formulation. This strategy led to increased intracellular uptake compared to free DOX. Consequently, assessments of cytotoxicity against OS MG-63 cell lines demonstrated that these nanoparticles displayed superior cytotoxic effects on MG-63 cells compared to free DOX.

### Recent developments in systemic NPs-based drug delivery

NPs-based drug delivery systems have been shown to overcome several limitations associated with the existing therapeutic strategies and offer several advantages over systemic chemotherapy for the treatment of OS<sup>12,18,54</sup>. These include efficiency in carrying high drug payloads, extending the drug's half-life, minimizing toxicity, and effectively tackling issues related to drug solubility and stability. Recent advancements in

nanoparticle-based drug delivery have focused on achieving more efficient and targeted drug delivery. This section will discuss these advancements, including targeted drug delivery, responsive drug delivery, and co-delivery systems.

Various NPs have been developed for targeted treatment of bone cancer to target the cancerous cells and minimize cytotoxicity to normal cells. In addition, nanocarriers with stimuli-responsive properties have been designed to release drugs in response to internal or external triggers, preventing premature drug release and ensuring precise drug delivery<sup>45,55</sup>. Co-delivery drug systems enable the simultaneous administration of multiple agents, leading to synergistic improvements in treatment effectiveness and reduced drug resistance<sup>38,56</sup>, (Fig. 3).

**Targeted NPs.** The commonly adopted approaches for targeting OS can be classified into three broad categories: organ-targeted therapy, cell-targeted therapy, and molecular-targeted therapy. In the realm of OS organ-targeted therapy, the most frequently employed strategy involves specifically binding to HAp, which is the principal component of bone tissue<sup>55,57-60</sup>, (Table 1).

Bisphosphonates are commonly utilized as bone-targeting ligands due to their exceptional ability to bind to HAp. To enhance their therapeutic potential, bisphosphonate-functionalized HAP NPs loaded with the chemotherapeutic agent JQ1 have been developed<sup>57</sup>. In vitro studies evaluating these NPs in both 2D, and 3D OS models have demonstrated their selectivity, as they showed increased toxicity towards murine OS K7M2 cells, compared to primary fibroblasts. Alendronate is another bone target ligand that belongs to the family of bisphosphonate. In a recent study<sup>59</sup>, liposomes were modified with both alendronate and low molecular-weight heparin to facilitate the delivery of DOX. The resulting NPs were evaluated using orthotopic K7M2 OS and bone metastasis cancer models. The results showed remarkable suppression of tumor growth and inhibition of tumor metastasis. In another study<sup>61</sup>, nanoclusters decorated with alendronate and loaded with DOX were synthesized. The targeting ability of these nanoclusters was evaluated using an in vitro bone cancer model, and their affinity to HAp was assessed based on DOX binding efficiency. Results indicated that the targeted nanoclusters exhibited approximately five-fold higher affinity compared to untargeted nanoclusters. Furthermore, compared to unmodified nanoclusters, the developed nanoclusters demonstrated enhanced accumulation within tumors in an orthotopic mouse model with intratibial injection of human OS HOS/MNNG cells.

Aptamers are short, chemically synthesized, single-stranded DNA and RNA oligonucleotides or polypeptide fragments that, upon folding, attain unique three-dimensional structures and bind to their target via structural recognition in a manner like an antibody-antigen interaction. Several

**Table 1 | Examples of osteosarcoma-targeted strategies used in drug delivery NPs**

NPs Types	Composition	Ligands	Targets	Size (nm)	Encapsulated Therapeutic agents	Encapsulation efficiency	Tested models	Study et al.
Lipid-polymer NPs	PLGA, DSPE-PEG-Mal and soybean lecithin	CD133 and EGFR aptamers	CSOs	110.2 ± 12.1	Salinomycin	66.5 ± 6.5	In vitro: Saos-2 and MG-63 OS cells; Saos-2 subcutaneous tumor in nude mice	62
Lipid-polymer NPs	PLGA, DSPC, DSPE-PEG-Mal and chol	CD133 aptamers	OS initiating cells	125.2 ± 9.9	ATRA	86.4 ± 5.6	In vitro: Saos-2 and U-2 OS cells; Saos-2 and U-2 OS subcutaneous tumor in BALB/c mice	63
Ceramic-based NPs	HAp	medronate	HAp	-30.5	QJ1	25.1	2D and 3D K7M2 OS in vitro models	57
Polymeric NPs	PDA	ALN	HAp	290.6 ± 2.2	PTX	80.32	In vitro: K7M2wt OS cells; K7M2wt OS subcutaneous tumor in BALB/c mice	55
Polymeric micelles	HA-C <sub>18</sub>	ALN	HAp	118 ± 3.6	CUR	N.A.	In vitro: MG-63 OS cells and HOB cells; MG-63 subcutaneous tumor in nude mice	156
Liposomes	SPC, chol, DDAB and S-PEG100	ALN	HAp	106.5 ± 3.5	DOX	94.2 ± 1.8	In vitro: K7M2 cells, 4T1 cells and RAW264.7 cells; orthotopic K7M2 OS model and bone metastasis cancer model	59
Polymeric NPs	PCL <sub>47</sub> -b-P[ <i>Gluc</i> -stat-( <i>Glu</i> -ADA) <sub>16</sub> ]	Glu and Glu-ADA	Bone	219	DOX	50.5	In vitro: U2OS cells	60
Metallic NPs	AF-NCC/Fe <sub>3</sub> O <sub>4</sub>	Folic acid	Folate receptor	23.86	DOX	99.6	In vitro: Saos-2 cells; toxicity study using BALB/c mice	66
Metallic NPs	Fe <sub>3</sub> O <sub>4</sub>	Folic acid	Folate receptors	103	DOX	85.1	In vitro: MG-63 cells and lung cancer A549 cells	65
Liposomes	SPC, chol, cationic lipid DOTAP, DOPE and Chol-SS-mPEG or Chol-mPEG	HA	CD44 receptor	165.3 ± 0.2	DOX	91.3 ± 3.2	In vitro: MG-63 cells and liver cells LO2; MG-63 subcutaneous BALB/c nude mice	69
Liposomes	SPC and chol	ALN-HA	Bone and CD44 receptor	173.1 ± 3.51	DOX	89.1 ± 0.4	In vitro: MG-63 cells; MG-63 orthotopic BALB/c nude mice	67
Liposomes	DSPC, chol and mPEG2000-DSPE	HA	CD44 receptor	204 ± 2	DOX	91.3 ± 3.1	In vitro: K7M2 OS cells and U-2OS OS cells	68
Liposomes	DPPC:chol and DSPE-PEG	YSA	EphA2 receptor	88	DOX	85.94	In vitro: Saos-2 and primary bone cells	73
Liposomes	DOTAP, chol, DPPC and DSPE-PEG	YSA	EphA2 receptor	109	DOX and siRNA	90	In vitro: Saos-2 and MG-63 cells	72
Polymeric NPs	mPEG-NH <sub>2</sub> , LP NCA and LC NCA	STP	Vimentin	85.9±5.5	Shikonin	N.A.	In vitro: Human osteoblast hFOB1.19 and OS 143B cells; 143B Intratibial BALB/c nude	71
Polymeric NPs	mPEG-NH <sub>2</sub> , LP NCA, LC NCA and DMF	STP	Vimentin	104.2 ± 52.8	DOX	29.70 ± 2.03	In vitro: 143B OS cells; 143B orthopedic BALB/c nude	70
Polymeric micelles	PEG-PTMC	RGD	to αvβ3 and αvβ5 integrins	46 to 73	DOX	57.3-73.4	In vitro: MG-63 cells	74

DSPE-PEG-Mal 1,2-distearoyl-sn-glycero-3-phosphoethanolamine-N-(maleimide (polyethylene glycol)-2000, Chol cholesterol), CSCs Cancer stem cells, DSPC 1,2-distearoyl-sn-glycero-3-phosphocholine, ATRA all-trans retinoic acid, PDA polydopamine, ALN: alendronate, PTX paclitaxel, HA-C<sub>18</sub>: amphiphilic copolymer hyaluronic acid-octadecanoic acid, CUR curcumin, HOB human osteoblasts, SPC soybean phosphatidylcholine, SPEG100 PEG-100 stearate, DDAB dimyristoylphosphatidylcholine, AF-NCC/Fe<sub>3</sub>O<sub>4</sub>: amine-functionalized nanocrystalline cellulose coated magnetic NPs, HA hyaluronic acid, DOTAP 1,2-dioleoyl-3-trimethylammonium-propan, DOPE 1,2-dioleoyl-sn-glycero-3-phosphoethanolamine, DSPC, 1,2-distearoyl-sn-glycero-3-phosphocholine, mPEG2000-DSPE 1,2-distearoyl-sn-glycero-3-phosphoethanolamine-N-[amino (polyethylene glycol)-2000], DPPC Dipalmitoylphosphatidylcholine, mPEG-NH<sub>2</sub> amino-terminated mPEG, LP NCA L-phenylalanine N-carboxyanhydride, LC NCA L-cystine N-carboxyanhydride, DMF dimethylformamide, PEG-PTMC poly(ethylene glycol)-block-poly (trimethylene carbonate).

aptamers have been developed against a variety of cancer targets, including extracellular ligands and cell surface proteins. These aptamers can serve as mediators between chemotherapeutics-loaded NPs and cancer cells. CD133 has been identified as a marker for cancer stem cells (CSC) in OS, resulting in the utilization of CD133 aptamers in OS-targeted drug delivery carriers<sup>22,62,63</sup>. Epidermal growth factor receptor (EGFR) has been found to be overexpressed in OS cells. Accordingly, to achieve dual targeting for both OS CSC and cancer cells, Chen et al.<sup>62</sup> created NPs containing salinomycin labeled with both CD133 and EGFR aptamers. The results indicated that the targeted NPs showed increased cytotoxicity in both OS cells and CSC, surpassing the effectiveness of single targeting or non-targeted delivery methods. In vivo studies using a mouse model with subcutaneously injected human OS Saos-2 cells also showed that the administration of the targeted NPs resulted in the best inhibition of tumor growth in compared to other controls.

The molecular-targeted therapy is considered the most specific targeting strategy; it targets sites such as protein molecules, including receptors, peptides, or gene segments that are highly upregulated in tumor cells. Folic acid, Hyaluronic acid (HA), and peptides have been reported to be used as targeting ligands decorated in the nanocarriers for OS-targeted drug delivery systems. Recent studies have demonstrated the potential of utilizing the folate receptor for targeted drug delivery, as these receptors are frequently overexpressed in multiple cancers, including OS<sup>64–66</sup>. Karimian et al.<sup>66</sup> fabricated magnetic NPs loaded with DOX and grafted with folic acid, targeted against folate receptors. The results showed an enhanced targeted delivery and internalization of the modified NPs, leading to improved therapeutic effects of DOX on OS Saos-2 cells. HA, a biocompatible endogenous polysaccharide, acts as a key ligand for CD44 cell surface receptors, which are abundant in OS cells<sup>67</sup>. To target these receptors, NPs, especially liposomes modified with HA, have been studied<sup>67–69</sup>. A recent study by Gazzano et al.<sup>68</sup> involved conjugating HA with H<sub>2</sub>S-releasing DOX-loaded liposomes. The results showed improved drug delivery and efficacy in vitro and compared to free drug and untargeted NPs. Peptides, including STP, RGD, and YSA, have been utilized to design NPs for targeted delivery to OS cells. STP has a specific affinity for vimentin, an overexpressed protein on the surface of various cancer cells, including OS cells<sup>70,71</sup>. An STP-decorated disulfide crosslinked polypeptide nanogel was fabricated for the targeted delivery of shikonin<sup>71</sup>. These NPs selectively accumulated in orthotopic 143B OS tumors, specifically recognizing vimentin on the cell membrane. This resulted in significant antitumor efficacy and inhibition of pulmonary metastasis. The 12-amino acid peptide, YSA, functions as a ligand for the EphA2 receptor, a surface molecule that is highly upregulated in OS cells<sup>72,73</sup>. In vitro studies<sup>73</sup> on DOX-loaded liposomes modified with YSA showed that the YSA-modified liposomes could efficiently target OS Saos-2 cells. This led to a higher therapeutic index of the prepared formulation compared to free DOX. RGD, a peptide with high cellular affinity, can bind to  $\alpha v\beta 3$  and  $\alpha v\beta 5$  integrins that are present on OS cells such as MG-63 and MNNG/HOS. In vitro studies<sup>74</sup> have shown that RGD-modified polymeric micelles have improved uptake into cells, specifically targeting OS MG-63 cells.

While targeted NPs offer great potential for treating OS, they face several challenges. For example, NPs designed to target OS using bisphosphonate ligands tend to accumulate in bone rather than specifically targeting malignant OS cells. Additionally, the extended presence of bisphosphonates in bone tissue may hinder osteoclast activity and disrupt bone homeostasis<sup>75</sup>.

Furthermore, in the realm of cell- and molecular-targeted NPs for OS, most are still in the experimental phase. There's a considerable transitional period before they can be clinically available due to numerous challenges. These challenges include the increased cost associated with ligand conjugation, potential alterations in NPs and ligand properties post-conjugation, and the need to identify suitable tumor markers or receptors for targeting.

**Stimuli-responsive drug-releasing NPs.** One of the prevalent challenges associated with conventional NPs is the premature release of their cargo before reaching their intended target site. Consequently, recent efforts have been dedicated to the design of modified nanocarriers capable of releasing their loaded drugs in response to various internal or external stimuli. Internal stimuli include differences in pH, redox potential, or enzyme concentrations. These triggers offer promising opportunities for responsive drug delivery systems, particularly in light of the distinct microenvironment found in tumor tissues compared to normal cells. Tumor microenvironments often feature acidic pH, elevated levels of glutathione (GSH) within the cellular cytoplasm, and the overexpression of specific enzymes. In addition to internal stimuli, external factors such as light, magnetic fields, temperature, and ultrasound have been explored. Various NPs systems, including liposomes, polymeric micelles, lipoplexes, and polyplexes, have been engineered to exploit these physical and chemical cues to fine-tune drug release. In the subsequent sections, we present an overview of the most extensively investigated environmentally responsive NPs<sup>69,76–78</sup>, (Table 2).

Redox-responsive NPs. GSH is a highly potent antioxidant and reducing agent in living cells. The concentration of GSH in the normal cellular cytoplasm is significantly higher than in extracellular fluid tissues (approximately 100-fold higher). Most remarkably, research has revealed that the concentration of GSH in cancer cells can be fourfold or more than that in normal cells<sup>69</sup>. Thus, the introduction of redox-responsive agents, such as disulfide bonds, diselenide bonds, and ditelluride linkages, has enabled the development of redox-responsive NPs<sup>79,80</sup>. These NPs can degrade within cancerous cells, facilitating the release of their cargo.

Disulfide bonds can be intracellularly cleaved by GSH in cancer cells, making them extensively used in the design of reduction-sensitive NPs. In research on redox-responsive NPs for OS, studies primarily focus on NPs with disulfide bonds<sup>23,67,69,81</sup>. Yin et al.<sup>23</sup> prepared reduction-responsive liposomes by attaching chitooligosaccharides (COS) to their surface through a disulfide linker. These reduction-sensitive liposomes, designated as Chol-SS-COS/DOX, exhibited stability under physiological conditions but underwent destabilization when exposed to reducing agents. Also, in the presence of GSH, the DOX release from Chol-SS-COS/DOX was accelerated compared to its release in the absence of GSH. In vitro, cytotoxicity study showed that reduction-sensitive liposomes showed higher cytotoxicity and more efficient internalization than non-reduction-sensitive liposomes in MG-63 cells. Moreover, the reduction-sensitive liposomes demonstrated a strong inhibitory effect on tumor growth in MG-63 cell-bearing nude mice and extended animal survival rates.

pH-responsive NPs. The pH in the bloodstream is around 7.4, while solid tumors including OS have an acidic extracellular environment with pH values ranging from 6.4–6.8<sup>82,83</sup>. The acidic cellular environment exhibits even lower pH values, such as pH around 5.5–6.0 in endosomes and pH around 4.5–5.0 in lysosomes<sup>84</sup>. The difference in the pH values between physiological conditions (e.g., blood) and tumor microenvironment, as well as between different cellular compartments, have been utilized for developing pH-responsive NPs that deliver drugs to the tumor tissues at both tissue and cellular levels.

Incorporating acid-sensitive linkers, such as acetal, hydrazone, glycerol ester, and amide groups, facilitates the conjugation of antitumor drugs to NPs. These linkers allow for the binding and stabilization of drugs to NPs under physiological pH conditions while subsequently permitting drug release within an acidic environment<sup>85</sup>. Meshkini et al.<sup>86</sup> synthesized mesoporous zinc HAp (ZnHAp) decorated with a pluronic block copolymer, F127, and subsequently, they conjugated MTX onto the surface of the NPs through an amide bond. They investigated the release of MTX from the NPs under different pH values ranging from 4 to 7.4 in the presence of crude protease from bovine pancreas. The results revealed that a larger amount of MTX was released at pH 4 as it has the highest concentration of the active

**Table 2 | Examples of stimuli-responsive NPs used for osteosarcoma therapy**

NPs	Composition	Stimuli	Size (nm)	Encapsulated drugs	Drug Encapsulation efficiency (%)	Tested models	Study et al.
Ceramic-based NPs	Aragonite	pH	20–80	DOX	Above 99	In vitro: Rat UMR-106 OS cell line and hFOB	77
Polymeric NPs	CaCO <sub>3</sub> -crosslinked HA	pH	~88.5	DOX	N.A.	In vitro: K7 murine cells: K7 OS -allografted BALB/c mouse	45
Ceramic-based NPs	ZSM-5 /CS NDs	pH	~300	DOX	97.7	In vitro: MG-63 cells In vivo: normal rat	88
Polymeric NPs	CD-coated magnetic NPs	pH	687.8 ± 17.4	MTX	89.2	In vitro: Saos-2 cells	89
Ceramic-based NPs	ZnHAP	pH	174.74 ± 0.227	MTX	N.A.	In vitro: Saos-2 cell	86
Liposomes	SPC, Chol and COS	Redox	105.7 ± 0.42	DOX	85.4 ± 1.36	In vitro: MG-63 OS cells and liver cell strain LO2 cells: MG-63 subcutaneous tumor in a BALB/c nude mouse model	23
Polymeric NPs	mPEG-PLG (DNs)	Redox	~154	IRN	57.5	In vitro: K7 OS cells: K7 subcutaneous t tumor in BALB/c mice	157
Polymeric NPs	PEG	Redox	62.5 ± 1.3	UA	N.A.	In vitro: MG-63 cells	81
Metallic NPs	gold core mesoporous silica NPs	Redox	~174.1	DOX	N.A.	In vitro: HUVEC, RAW264.7 and 143B cells: orthotopic 143B tumor model	78
Polymeric NPs	γ-polyglutamic acid (γ-PGA)	Redox	100.5 ± 0.131	MTX	N.A.	In vitro: 143B cells	158
Ceramic-based NPs	Silica	Light	~130	Topotecan	N.A.	In vitro: HOS cells	91
Polymeric micelles	Poly DOX micelles	Light	~27	DOX	N.A.	In vitro: K7M2wt OS cells In vivo: K7M2wt subcutaneous tumor in BALB/c mice	92
Ceramic-based NPs	silica-coated bismuth sulfide	Light	~120	DOX	99.85	In vitro: UMR-106 OS cells: UMR-106 subcutaneous tumor in BALB/c mice	93

hFOB human fetal osteoblastic cell line, PAA polyacrylic acid, CaCO<sub>3</sub> calcium carbonate, HA hyaluronate, ZSM-5 /CS NDs mesoporous ZSM-5 zeolites/chitosan core-shell nanodisks, CD cyclodextrin, ZnHAP mesoporous zinc hydroxyapatite, SPC Soybean phosphatidylcholine, chol cholesterol, COS chitoooligosaccharides, mPEG-PLG (DNs) polymer SO<sub>2</sub> prodrug, synthesized through coupling of a small-molecule SO<sub>2</sub> donor, N-(3-azidopropyl)-2,4-dinitrobenzenesulfonamide to the side chains of methoxy poly(ethylene glycol)-block-poly(γ-propargyl-L-glutamate) block copolymer, IRN irinotecan, UA Ursolic acid, PEG polyethylene glycol.

protease that's most likely responsible for the cleavage of MTX from the NPs.

Calcium carbonate (CaCO<sub>3</sub>) exhibits remarkable pH sensitivity as it undergoes dissociation in acidic solutions, making it a versatile choice for various controlled-release applications. CaCO<sub>3</sub> serves both as a nanocarrier for antitumor drugs and as a crosslinker between NPs and therapeutic agents<sup>45,77</sup>. Fu et al.<sup>77</sup> fabricated aragonite (CaCO<sub>3</sub> polymorph) NPs loaded with DOX. These NPs exhibited a pH-sensitive pattern, with 36% of DOX released in a PBS solution (pH 7.4) within the first 2 h and approximately 80% of DOX released within 24 h. While at acidic PBS buffer (pH 4.8), around 72% of DOX was released at the first hour, and about 90% was released within 8 h. Zhang et al.<sup>45</sup> fabricated DOX-loaded HA NPs that were further crosslinked to CaCO<sub>3</sub>, to enhance their stability and make the NPs sensitive to the acidic tumor microenvironment. They demonstrated that the amount of DOX released at pH 6.8 and 5.5 was 2.2 and 4.1 times higher than the neutral conditions (7.4), respectively. They also evaluated the biodistribution and antitumor efficacies of the developed NPs in both primary and advanced models of murine OS, compared with non-crosslinked NPs (HA-DOX) and free DOX, the HA-DOX/CaCO<sub>3</sub> showed effective tumor accumulation and highest tumor inhibition efficacy.

In acidic conditions, the amino groups present in chitosan can become protonated. This property enables chitosan to function as a pH-responsive polymer, which has been utilized in previous studies for the functionalization of NPs<sup>76,87,88</sup>. Yang et al.<sup>88</sup> prepared mesoporous ZSM-5 zeolites/chitosan core-shell nanodisks loaded with DOX (ZSM-5/CS/DOX). The CS layer on the nanodisks was used to regulate the DOX release, exhibiting pH-responsive behavior with a higher drug release rate in a slightly acidic environment compared to the neutral environment. Results demonstrated a pH-dependent release of DOX from the nanodisks. At normal physiological conditions (pH 7.4), the DOX cumulative release ratio from the ZSM-5/CS/DOX nanodisks was only 39.9% after 7 days of incubation. In contrast, when the pH decreased to 5.5, 71% of DOX was released. In addition, the therapeutic effects of the ZSM-5/CS/DOX nanodisks were studied with both in vitro and in vivo tests. Compared to the free DOX group, the mesoporous ZSM-5/CS/DOX group exhibited more effective MG-63 cells suppression with lower side effects.

The ionic interaction between the loaded drug and its carrier may provide a pH-sensitive property to the delivery system. Ahmadi et al.<sup>89</sup> developed NPs consisting of a magnetic inner core and polymeric outer shell with cationic moieties to deliver MTX (MTX/Cat-MN) to the Saos-2 cells. The MTX release profiles from the nanocarriers were next evaluated under

various pH solutions 5.0 and 7.4. At pH 7.4, the cumulative amount of released MTX from MTX/Cat-MN was  $44.21 \pm 2.98\%$  after about 12.5 days. In contrast, under acidic conditions (pH 5.0), MTX/Cat-MN could release up to  $72.73 \pm 3.19\%$  of total encapsulated MTX. Under low pH values, the carboxylate anion of MTX was protonated. This leads to the impairment of the electrostatic interactions between MTX and the Cat-MN protonated functional groups. Consequently, this can be the reason for the acceleration of the MTX release.

While certain pH-responsive or redox-responsive nanoparticles exhibit promising performance *in vitro*, they may be restricted by the complex physiological or pathological environment *in vivo*. Primarily, these responsive nanoparticles struggle to precisely regulate cargo release at tumor sites within optimal time frames and dosages. Moreover, their functionality may be impeded by the limited availability of stimulus factors *in vivo*. Additionally, the response kinetics *in vivo* are unpredictable due to the influence of various factors.

**Light-responsive NPs.** Light is an example of an external stimulus for drug delivery systems; it is quite beneficial due to its non-invasive nature and precise facilitation of spatiotemporal drug release. Light used in photo-responsive drug delivery nanocarriers can be categorized into three primary ranges: ultraviolet (100–400 nm), visible (400–700 nm), and near-infrared (700–1000 nm) light. Light within the 300–700 nm range is typically harnessed for applications involving superficial tissues, while near-infrared (NIR) light, with longer wavelengths, is employed for deeper tissue penetration<sup>90</sup>.

Martínez-Carmona et al.<sup>91</sup> developed a visible light-responsive drug delivery system using mesoporous silica NPs loaded with topotecan, a chemotherapy drug. Porphyrin nanocaps blocked the pore outlets of the NPs via ROS-cleavable linkages. Upon exposure to visible light, the porphyrin nanocaps generated ROS that breaks the bonds and uncaps the pores, releasing 99% of the loaded drug after 18 h after being subjected to 30 min of low-intensity light irradiation. *In vitro* tests on OS HOS cells showed controlled release of topotecan and induced toxicity within the cancer cells. In another study, Chen et al.<sup>92</sup> created a DOX-conjugated polymer that can self-assemble into polymeric micelles (Poly-Dox-M) in water and is responsive to UV light. When exposed to UV light, the bond in the micellar polymer structure breaks, leading to a rapid release of DOX at the target tumor site. Recently, NIR-Responsive mesoporous silica-coated bismuth sulfide NPs encapsulating DOX were developed<sup>93</sup>. These NPs demonstrated NIR-sensitive drug release, even under a very low power density of  $0.3 \text{ W cm}^{-2}$ .

The efficacy of light-responsive nanoparticles in treatment is impeded by the limited depth of light penetration. Visible and UV light (up to 700 nm) can only permeate biological tissues to a shallow extent, typically a few millimeters, due to strong scattering and absorption by soft tissues. Consequently, the utilization of Visible and UV light is confined to superficial tissues. While NIR light allows for deeper tissue penetration, reaching depths of up to a few centimeters, it may still fall short in reaching bone tissues situated deep within the body.

**Co-delivery of drugs using NPs.** Multidrug resistance (MDR) of tumors poses a major challenge to chemotherapy efficacy and contributes to cancer recurrence. This phenomenon is attributed to ATP-binding cassette (ABC) transporters such as P-glycoprotein, which efflux drugs from cancer cells. To overcome MDR, researchers have explored the use of polychemotherapy, which involves the concurrent administration of drugs with distinct mechanisms of action<sup>94</sup>. Recently, the co-delivery of drugs via nanoplateforms has gained significant attention as a promising avenue for tackling MDR<sup>95</sup>. Caliskan et al.<sup>96</sup> developed a liposomal formulation co-encapsulating Gemcitabine (GEM) and Clofazimine (CLF). The hydrophilic core of the liposomes encapsulated GEM, an anticancer agent that disrupts DNA synthesis, while CLF, a lipophilic agent that inhibits Wnt signal transduction, was loaded in the lipid bilayer. This co-loading approach showed a synergistic effect *in vitro*, resulting in greater

cytotoxicity than individual liposomal treatments of either GEM or CLF. A recent investigation<sup>94</sup> employed the formation of lipid-polymer hybrid NPs loaded with both DOX and Edelfosine. Evaluations demonstrated a marked enhancement in the anticancer efficacy of the dual drug-loaded NPs and suppression of tumor growth without any observable adverse effects.

Combination therapy is not restricted to chemotherapeutic agents alone. It can also involve a combination of chemotherapeutics and proteins or other therapeutic agents. Some proteins can offer unique advantages over chemotherapeutics, including inherent bioactivity, high functional specificity, and reduced side effects. This synergistic combination of chemotherapeutics and proteins can lead to improved therapeutic outcomes and reduced side effects in cancer treatment<sup>97</sup>. A recent study<sup>38</sup> has demonstrated the development of calcium carbonate mineralized NPs loaded with the therapeutic protein cytochrome c and the chemotherapeutic agent DOX. The NPs were evaluated both *in vitro* using mouse OS K7 cells and *in vivo* with a K7 orthotopic OS mouse model. The results showed a significant improvement in biocompatibility and enhanced synergistic anti-OS effects compared to control groups. In a recent study, Hu et al.<sup>98</sup> investigated the potential of selenium-doped calcium phosphate NPs loaded with DOX. Selenium, a trace element with potential antitumor effects, enhances the intracellular level of ROS and contributes to overcoming MDR by down-regulating ABC transporter proteins, leading to the apoptosis of cancer cells. The developed NPs effectively downregulated the expression of MDR-related proteins in the ABC family and reversed MDR in OS cells. *In vivo* studies confirmed the efficacy of these NPs, demonstrating significant induction of tumor apoptosis, suppression of tumor growth, and reversal of MDR.

Zhang et al.<sup>11</sup> created a crosslinked nanogel utilizing HA to co-deliver CDDP and DOX. Both drugs interact with DNA and cause damage, which is part of their anticancer mechanism. CDDP served not only as a supplementary anticarcinogen but also as a crosslinker, preventing premature release of DOX and thereby enhancing the synergistic therapeutic effects. The CDDP crosslinked DOX-loaded nanogel exhibited optimized biodistribution, elevated antitumor efficacy, and reduced multi-organ toxicity compared to free drugs and their combination using a K7 subcutaneous OS mouse model.

### Limitations and challenges

As discussed previously, NPs-based drug delivery systems have emerged as a promising approach to address the limitations of systemic drug administration and have made significant progress in paving their way into clinical practice. These NPs offer distinct advantages over traditional chemotherapy, including a significant reduction in adverse effects, improvements in drug pharmacokinetics, and extended circulation time in the bloodstream<sup>99,100</sup>. Despite the substantial progress made in developing NPs for cancer treatment, several challenges and limitations persist. NPs are typically administered intravenously to ensure direct access to the bloodstream; however, this method often results in rapid NPs clearance, limiting their effective interaction with target sites. More than 95% of systemically injected drugs tend to accumulate in organs such as the liver, spleen, and lungs, with less than 5% reaching the targeted tumor site, even with advanced strategies like coupling targeting ligands or designing stimuli-responsive release mechanisms<sup>101,102</sup>. This challenge is even more pronounced in delivering drugs to bone tissue due to the highly mineralized extracellular matrix of bone, which impedes the diffusion of molecules from the bloodstream into the bone tissue. Consequently, higher NP dosages are required, leading to increased drug concentrations and potentially greater toxicity<sup>103</sup>.

### Local drug delivery

Recently, local administration of chemotherapy approaches has drawn much attention, offering significant benefits over systemic drug delivery, especially for bone cancer treatment. This strategy bypasses the limitations that impede the NPs in the bloodstream before reaching the target site.

These limitations include short blood circulation time, clearance by Kupffer cells, low local concentrations, and limited accumulation in target tissue. By directly delivering drugs locally to the target site, local administration enables higher drug concentrations at the desired location, resulting in lower systemic toxicity and enhanced therapeutic efficiency.

Local delivery of chemotherapeutics can be achieved through different approaches, such as implanting nanocarriers, injecting hydrogels, and implanting scaffolds (see Fig. 4).

### Implantable nanocarriers

To enhance the efficiency of NPs delivery, recent research has shifted from intravenous injection to local delivery directly at the tumor site. This enhancement is achieved by implanting the NPs in a precise and localized intratumoral delivery manner<sup>44,104-106</sup>. In OS studies, implantable NPs primarily involve HAP NPs injected locally near the tumor in murine models.

A ternary nanodrug delivery system consisting of HAP, bovine serum albumin (BSA), and the chemotherapy agent PTX was prepared for the locoregional treatment of OS<sup>104</sup>. The efficacy of this complex was evaluated using an orthotopic OS mouse model. Results showed that the ternary NPs

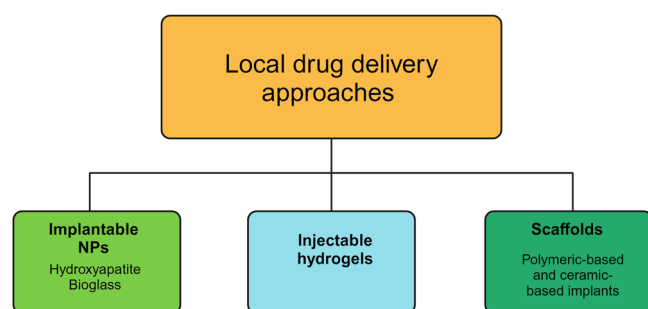


**Fig. 4 | Common strategies for local delivery of anticancer agents.** Various approaches for local delivery of chemotherapeutics include the use of implantable nanocarriers, injectable hydrogels, and implantable scaffolds. Created with BioRender.com.

exhibited superior anticancer effects compared to control groups, which consisted of bare PTX drug and HAP-BSA NPs. Additionally, the ternary nanodrug delivery system effectively inhibited the metastasis of the tumor to other organs. Recently, Liu and his team<sup>44</sup> demonstrated the efficacy of local delivery of DOX via implantable HAP particles. In a mouse model of aggressive OS induced by subcutaneous injection of aggressive human OS 143B cells, they demonstrated that the local delivery of DOX via HAP particles resulted in a more pronounced tumor eradication effect compared to systemic administration (Fig. 5). Additionally, combining micro HAP particles in a carrier with nano HAP particles improved biocompatibility and safety by ensuring that the nano Hap particles were retained locally within the tumor site.

### Injectable hydrogels

The utilization of hydrogel-mediated local drug delivery systems has gained increasing interest in recent years due to several advantages. These systems exhibit ease of injectability and a mild gelation process, as well as reduced systemic toxicity. Moreover, hydrogels can be administered directly at the tumor site via a syringe, simplifying the delivery process. Their highly porous structure can be finely tuned by adjusting the density of cross-links in the gel matrix and the hydrogels' affinity for the aqueous environment in which they are swollen. This porosity facilitates the incorporation of drugs into the gel matrix through straightforward physical mixing. The release of drugs from hydrogels depends on factors such as water content, pore size, and the diffusion coefficient of the drug molecules. Typically, hydrogels with high water content and large pore sizes exhibit relatively rapid drug release, spanning from a few hours to several days<sup>107</sup>.

Triblock copolymer PLGA-PEG-PLGA, an injectable thermosensitive hydrogel, has gained widespread recognition as a potent drug local delivery vehicle due to its good injectability, biodegradability, and biocompatibility<sup>108,109</sup>. In a study by Yang et al.<sup>109</sup>, the efficacy of a PLGA-PEG-PLGA-based hydrogel as a delivery vehicle for DOX was investigated in a K7 subcutaneous OS mouse model. The results indicated a remarkable improvement in the maximum tolerated dose of DOX, which was two-fold higher than that of the intravenous injection of free DOX. Additionally, the localized administration of DOX via the hydrogel did not result in obvious

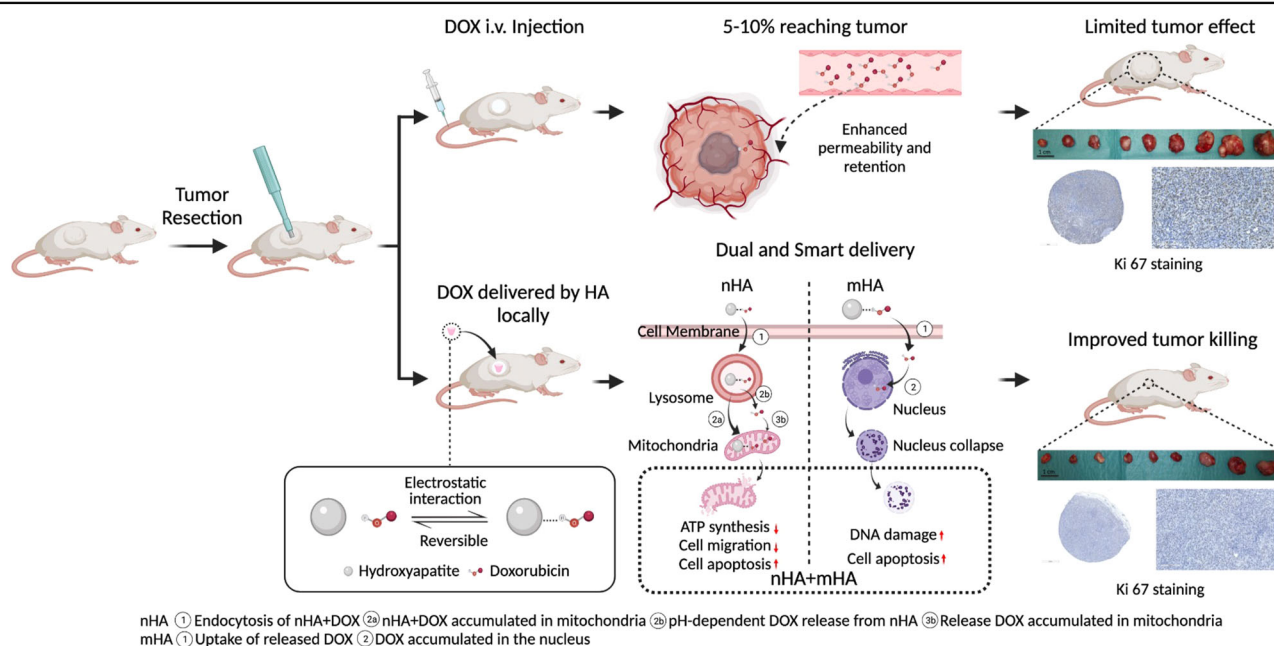


**Fig. 5 | Comparing the efficiency of DOX delivery through local HAP particles and systemic injection.** A schematic illustration showing the efficiency of doxorubicin (DOX) delivery via locally implanted HAP particles compared to systemic injection. Intravenous injection results in only 5–10% of DOX accumulating in the

tumor, leading to limited therapeutic effect. In contrast, local delivery through HAP particles achieves a stronger tumor eradication effect. (Reprinted with permission from ref. 44).

systemic toxicity. In a recent study by the same group<sup>110</sup>, the efficacy of a PLGA-PEG-PLGA hydrogel was evaluated as a carrier for the delivery of a  $\beta$  cyclodextrin curcumin (CD-CUR) inclusion complex and DOX. The results obtained from the K7 subcutaneous OS mouse model indicated that the co-loaded hydrogel had a superior antitumor effect compared to free DOX + CD-CUR or single-drug treatments. Moreover, the localized treatment strategies demonstrated high systemic safety. In another study, Si et al.<sup>111</sup> synthesized PLGA-PEG-PLGA hydrogel encapsulated with both DOX and CDDP. The drug release profile from the hydrogel exhibited an initial burst release during the first two days, followed by a sustained release for more than 10 days. In a mice OS Saos-2 xenografts model, the co-loaded hydrogel exhibited superior efficiency in suppressing tumor growth compared to the administration of either the free drugs or single drug-loaded hydrogel, suggesting a synergistic anti-tumor effect. Importantly, the localized administration of different treatments did not result in any detrimental impact on other vital organs, indicating a low systemic toxicity.

Zheng and colleagues<sup>112</sup> introduced a hydrogel-based delivery system for the local administration of Combretastatin A-4, an antiangiogenic agent, and docetaxel, a chemotherapy agent. The system consists of injectable thermosensitive polypeptide hydrogel embedded with PLGA microspheres. Results from the K7 subcutaneous OS mouse model demonstrated that this co-loaded hydrogel effectively suppressed tumor growth, surpassing the efficacy of other formulations, including free drugs, a combination of free drugs, and single-drug-loaded hydrogels. Furthermore, through histopathology and immunohistochemistry analysis, the co-loaded hydrogel demonstrated a significant enhancement of antiproliferative effects and reduction of drug toxicity.

Hydrogels, despite their promising results in treating OS, face challenges due to their low tensile strength. This limitation hinders their use in load-bearing applications and can lead to premature dissolution or displacement from a targeted local site. Furthermore, hydrogels often fail because of poor mechanical and structural stability, which prevents them from maintaining complex structures.

### Scaffolds

The surgical resection of a bone tumor often leads to the formation of critical-sized bone defects that do not possess the innate capacity for spontaneous healing. Consequently, following the removal of a bone tumor, clinicians are thus faced with the challenge of addressing these defects, typically resorting the defect by implantation of biomaterial scaffolds. However, the conventional scaffolds employed in this context lack therapeutic capabilities to eradicate residual tumor cells. In light of this, there has been a growing interest in the development of localized drug delivery systems integrated within bioactive scaffolds<sup>113</sup>. These scaffolds not only aim to fill the post-surgical bone defect but also ensure the targeted local delivery of a high local concentration of chemotherapy. They are predominantly constructed from materials such as metal, bioceramics, biodegradable polymers, and composites.

### Drug loaded -scaffolds

**Metal.** Metals, including Ti and its alloys, stainless steels, Mg alloys, and other biodegradable metals, are primarily recognized for their exceptional mechanical strength. Titanium is extensively utilized in clinical applications, particularly for dental implants, and is also a preferred material for load-bearing applications<sup>113-115</sup>. However, Titanium implants often face challenges with poor osseointegration (lack of tissue adherence), leading to implant failure. One approach to address this issue is by manipulating the implant's surface topography. For example, Maher et al.<sup>114</sup> fabricated titanium implants with dual micro- and nanotopography to enhance bone integration. Additionally, these implants were loaded with two types of drugs, DOX and apoptosis-inducing ligands (Apo2L/TRAIL). In vitro studies demonstrated the implants' strong anticancer efficacy against cancer cells.

**Bioceramics.** Currently, bioceramic scaffolds, including materials such as calcium phosphates (specifically HAp and TCP), bioactive glasses, and

silicate-based bioceramics, are widely used in bone-related clinical settings. Their popularity stems from their ability to closely mimic the mineral phase of bone, making them conducive to excellent bone regeneration<sup>116,117</sup>. However, the main drawback of bioceramics is their intrinsic brittleness, which means they cannot withstand deformation without rupturing. This brittleness can lead to the sudden failure of the scaffold structure under load-bearing conditions.

Several recent studies have explored the use of polymers, such as PLGA, PCL, chitosan, and cyclodextrins, in conjunction with bioceramic bone scaffolds. These polymers are employed to regulate the release kinetics and mitigate the burst release of biomolecules or chemotherapeutics from the scaffolds<sup>118,119</sup>. In one notable investigation, Bischoff et al.<sup>118</sup> employed a coating of cyclodextrins on HAp, which served as a carrier for DOX. The findings revealed that the DOX released from the cyclodextrin-coated HAp demonstrated sustained biological activity, leading to prolonged and enhanced cytotoxic effects on both OS MG-63 cells and non-malignant cells (primary osteoblasts and endothelial cells) compared to biomaterials lacking cyclodextrin-loaded DOX. Furthermore, they evaluated the delivery system in a hypoxic environment (less than 1% O<sub>2</sub>), mimicking the initial conditions post-bone resection. The drug delivery system effectively inhibited cancer cell growth while preserving the viability and proliferation of healthy cells. In another study<sup>120</sup>, researchers employed 3D printing to create calcium phosphate cement (CPC) scaffolds with interconnected pores. These scaffolds were further enhanced by applying a stable coating of a model anticancer drug, 5-fluorouracil, using a combination of hydrophilic solutions of Soluplus and PEG polymer. Dissolution studies conducted in vitro demonstrated that nearly 100% of the drug was released within a span of 2 h, indicating a rapid release rate. Additionally, cell culture experiments utilizing two distinct cell lines exhibited a significant inhibition of cell growth, as evidenced by a significant reduction in cell numbers after a period of 5 days.

**Polymers.** Polymeric scaffolds can be made from either natural or synthetic polymers. Natural polymers include silk fibroin, collagen, gelatin, and fibrin. These polymers offer advantages such as biodegradability and bioactive properties, which enhance cellular interaction and performance within biological systems<sup>121</sup>. However, natural polymers are suboptimal for bone applications due to their low mechanical stability and lack of tunability in degradation rates.

Among synthetic polymers, PCL, polylactic acid (PLA), PLGA, and their derivatives are the most used. These materials are favored for their controllable biodegradability and ability to generate porous scaffolds. Biodegradable synthetic polymers can be synthesized through the manipulation and customization of their molecular structure. This biodegradability is achieved through molecular design, where certain polymers incorporate chemical bonds susceptible to hydrolysis when exposed to the body's aqueous environment<sup>122</sup>. Alternatively, some polymers degrade through cellular or enzymatic pathways. However, synthetic polymers also have limitations, such as the production of high local concentrations of acidic degradation products and the loss of mechanical strength after degradation.

In a recent study, Wang and colleagues<sup>123</sup> developed 3D biodegradable printed PLLA implants that were loaded with DOX, ifosfamide, and MTX for the treatment of OS. The drug delivery system exhibited several advantages, including localized chemotherapy, the capacity to deliver multiple drugs, and sustained drug release over an extended period.

**Scaffolds containing drug-loaded NPs.** Recent studies have explored the incorporation of drug-loaded NPs into scaffolds. This approach offers distinct advantages, primarily enhancing drug potency and stability while facilitating a controlled release of the encapsulated drug. Loading drugs onto NPs not only optimizes their efficacy but also ensures a more sustained and targeted delivery, contributing to the overall efficacy of the therapeutic intervention.

Liposomes have been commonly utilized as nanocarriers in numerous studies<sup>124,125</sup>. In a particular study<sup>125</sup>, liposomes loaded with Ruthenium were

integrated into a PCL scaffold. The findings demonstrated a relatively prolonged drug release over a 48-hour period. Furthermore, MTT assays were employed to assess MG-63 cell viability and apoptosis rates. The experimental results indicate that Ruthenium induces mitochondrial dysfunction, leading to apoptosis in MG-63 cells.

In a recent study<sup>126</sup>, the researchers explored the utilization of PLGA NPs loaded with DOX, which were then incorporated into CPC. The objective was to enhance the localized delivery of DOX and evaluate its cytotoxic effects on U2OS cells, both in monoculture and coculture with mesenchymal stem cells, in comparison to CPCs solely loaded with DOX. The findings revealed that the inclusion of PLGA-DOX NPs within the CPC matrix resulted in a more efficient release of DOX (80% of DOX released over 7 days), leading to elevated cytotoxicity levels in U2OS cells.

Jiang et al.<sup>127</sup> have developed 3D-printed gelatin-based scaffolds using a combination of polydopamine (PDA)-hybridized nanosized zeolitic imidazolate framework-8 (pZIF-8 nanoMOFs) and PDA-decorated-hydroxyapatite NPs. In both in vitro and studies, the researchers examined the effects of encapsulating the nanoMOFs with anti-cancer CDDP into the scaffolds. The findings demonstrated that the encapsulation of CDDP effectively inhibited tumor growth in a subcutaneous OS mouse model. Release studies have demonstrated that CDDP is released in response to the tumor microenvironment due to the pH and H<sub>2</sub>O<sub>2</sub> sensitivity of pZIF-8 nanoMOFs (with 50% of CDDP released after 5 days).

### Multifunctional scaffolds

**Multifunctional scaffold-based drug delivery systems.** Common bone scaffolds have served a dual purpose by efficiently filling critical-sized bone defects resulting from surgical bone tumor resection and also functioning as a reliable delivery system for chemotherapy and therapeutic agents. In contrast, the newly introduced multifunctional bone substitutes not only adeptly address filling and delivering but also introduce an additional function: actively promoting bone regeneration. This advanced category serves a triple purpose, addressing the following key aspects:

1. Fill- filling the critical-sized bone defect resulting from surgical restriction of the bone tumor.
2. Deliver – local administration of chemotherapeutic drugs, facilitating the elimination of any remaining tumor cells after surgery while minimizing potential side effects.
3. Repair – promoting bone regeneration and restoring bone defects.

For a scaffold to effectively promote bone regeneration, it should mimic the structure and function of natural bone and possess the following essential properties:

1. Biocompatibility: the scaffold must integrate with the native bone without inducing inflammatory reactions.
2. Mechanical strength: it should have mechanical properties that match those of the host tissue, providing adequate support<sup>128–130</sup>.
3. Biodegradability: the degradation rate of the scaffold should be synchronized with the bone regeneration process<sup>131</sup>.
4. High porosity and interconnectivity: a porosity of over 60%, with interconnected pores ranging from 100–500 μm, is optimal for encouraging cell attachment, migration, and ingrowth throughout the scaffold<sup>132</sup>.
5. Surface functional characteristics: the scaffold should have surface properties that promote cell adhesion and proliferation.
6. Osteoconductivity and osteoinductivity: osteoconductive scaffolds support the migration of bone-related cells, such as mesenchymal cells, osteoblasts, and osteoclasts. Osteoinductive scaffolds induce the differentiation of various cell types into osteogenic cells<sup>133</sup>.

Table 3 provides a summary of the latest scaffold developments used as delivery systems for OS treatment, highlighting their demonstrated potential in facilitating bone regeneration.

Several in vitro studies have introduced multifunctional scaffolds<sup>124,134–137</sup>. In one such study<sup>135</sup>, researchers engineered a chitosan/nHAp scaffold loaded with zoledronic acid (CS/nHAp/Zol). The resultant CS/nHAp/Zol scaffolds demonstrated the inhibition of giant cell tumors of bone growth in vitro. In addition, these scaffolds exhibited minimal toxicity toward human bone marrow mesenchymal stem cells. Furthermore, the CS/nHA/Zol scaffolds displayed osteoinductivity comparable to that of the CS/nHA scaffolds. In a separate study, Tan et al.<sup>134</sup> developed a composite scaffold comprising PLLA and nHAp, encapsulating the drug metformin. Surprisingly, metformin demonstrated dual functionality, acting as a tumor cell suppressor and a bone regeneration accelerator, depending on its concentration. The scaffolds effectively inhibited the proliferation of Saos-2 cells through apoptosis induction. Additionally, these scaffolds supported human bone marrow mesenchymal stem cell adhesion and proliferation, fostering osteogenesis throughout prolonged culture periods. In another study, Bose and colleagues<sup>119</sup> coated a TCP scaffold with PCL to evaluate the controlled release of vitamin C from the scaffold. The results revealed that the presence of PCL helps to reduce the burst release of vitamin C from TCP scaffolds during the first 24 h of release, leading to a more controlled and sustained release of vitamin C over 60 days. These scaffolds were found to enhance the proliferation, viability, and differentiation of human fetal osteoblast cells. Furthermore, preliminary in vitro study demonstrated that these scaffolds also inhibited the proliferation of OS cells.

In an in vivo study, Lu et al.<sup>138</sup> developed PDA-coated composite scaffold consisting of DOX-loaded lamellar HAp and PLGA (PDA@DH/PLGA). The PDA@DH/PLGA scaffold not only exhibited a significant inhibitory effect on OS MG-63 cell growth but also demonstrated enhanced adhesion and proliferation of osteoblasts during a 20-day drug release period. Preliminary assessment of in vivo osteogenesis using a mouse skull defect model revealed superior bone growth surrounding the PDA@DH/PLGA scaffold compared to the DH/PLGA scaffold without PDA coating after 20 days of drug release. In another in vivo study, Zhang et al.<sup>115</sup> engineered a porous titanium scaffold loaded with nano-HAp and implanted it in a critical-sized segmental bone defect within a VX2 tumor environment in a rabbit tumor model. The nano-HAp-releasing scaffold exhibited high efficacy in suppressing tumor growth and osteolytic lesions, concurrently promoting bone regeneration (Fig. 6).

**Multifunctional scaffold based on synergistic therapy.** In addition to drug-loaded scaffolds, another approach for addressing tumor cell residues and repairing bone defects involves photothermal therapy or magnetic fluid hyperthermia functionalized scaffolds<sup>139–142</sup>. Unlike drug-loaded scaffolds, these functionalized scaffolds utilize the high temperature generated by photothermal agents or magnetic NPs to eradicate tumor cells.

In photothermal therapy, the scaffolds contain photothermal agents that absorb NIR light radiation, converting it into localized heat. This elevated temperature, reaching up to 50 °C, effectively destroys tumorous cells. Conversely, in a magnetic fluid hyperthermia-based approach, the scaffold incorporates magnetic materials or introduces magnetic agents to a non-magnetic scaffold. The application of an external magnetic field generates heat locally within the bone defect. Studies have shown that temperatures ranging from 42 to 46 °C (moderate hyperthermia) are promising in bone cancer therapy, effectively eliminating cancerous cells without harming surrounding healthy tissue<sup>143–145</sup>.

Recent research has introduced a synergistic therapy combining drug-loaded scaffolds with photothermal therapy or magnetic fluid hyperthermia. This approach aims to achieve controlled release of the loaded anti-tumor drug upon increased temperature, providing an on-demand treatment strategy.

Yang et al.<sup>146</sup> developed porous scaffolds comprised of magnetic mesoporous calcium silicate/chitosan (MCSC) for synergistic chemophotothermal therapy (Fig. 7). Their findings demonstrate that NIR laser stimulation elevates temperature and facilitates DOX release from MCSC scaffolds, with a 24-hour cumulative release ratio of 79.3%, suggesting rapid

**Table 3 | Scaffolds based on drug delivery system for osteosarcoma treatment and their role in bone regeneration**

Scaffold material	Therapeutic agents	Loading approach/Cross-Linking Method	Release time	Role in promotion bone regeneration	Study type	Study et al.
TCP, HAp	DOX and CDDP	Physical entrapment	40 days ~52% of the DOX loaded in beads was released	N.A.	In vitro study MG-63 cells	159
Titanium	DOX and apoptosis-inducing ligand (Apo2L/TRAIL)	Physical entrapment	cumulative release of DOX and Apo2L/TRAIL after 6 h was 40% and 70%, respectively	N.A.	In vitro study MDA-MB-231-TXSA breast cancer cells and NIH 3T3 fibroblasts	114
CS, nHA	Zol	Physical adsorption	Almost no Zol releasing from the CS/nHA/Zol scaffolds	Adding of Zol into CS/nHA did not hamper the osteogenic differentiation, and the CS/nHA/Zol scaffolds presented good osteoinductivity the same as CS/nHA scaffolds	In vitro study GCT cells hBMSCs	135
Poly CD-coated HA	DOX	Physical adsorption	N.A.	N.A.	In vitro study MG-63 cells POBs HUVECs	118
PEEK	DOX	Physical adsorption	N.A.	N.A.	In vitro MG-63 cells	160
Titanium	nHA	Covalent immobilization/ coatings onto a scaffold surface	More than 11% of the total coated n-HA was released on day 7	nHA coating not only suppressed tumor growth but also promoted bone regeneration	In vitro study YX2 tumor cells and L929 fibroblasts critical-sized segmental bone defect in a rabbit tumor model	115
PCL coated TCP	vitamin C	physical entrapment	60 days	Release of vitamin C from PCL coated $\beta$ -TCP scaffolds has been shown to improve the proliferation, viability, and differentiation of osteoblasts	In vitro study hFOB MG-63 cells	119
TCP	Curcumin-loaded liposomes	physical entrapment	N.A.	The scaffolds exhibit no cytotoxicity toward healthy osteoblast cells, promoting adhesion and proliferation.	In vitro hFOB and MG-63 cells	124
m-SiO <sub>2</sub> / PCL	Ruthenium-loaded liposomes	physical entrapment	53% of Ruthenium after 48h	N.A.	In vitro MG-63 cells	125
PLLA	Mixture of DOX, ifosfamide, MTX, and CDDP	physical entrapment	12 weeks – examined in an animal model	N.A.	In vitro study U2OS cell line subcutaneous tumor in nude rat	123
CPC	5-fluorouracil	Physical adsorption	2 hrs	N.A.	In vitro study Hek293T and HeLa cells	120
CPC	PLGA NPs loaded with DOX	encapsulating NPs into scaffold	80% of DOX released over 7 days	N.A.	In vitro study U2OS cells	126
Sr, CS, HAp	NCTD	physical entrapment	N.A.	The composite biomaterial promoted the mineralization of osteoblasts effectively.	In vitro study MG-63 and MC3T3-E1 cells	137
Gelatin	BMP2-loaded pZIF-8 nanoMOFs CDDP-loaded pZIF-8 nanoMOFs polydopamine-decorated HA NPs	physical entrapment	50% of CDDP was released after 5 days. 40% of BMP-2 released after 21 days	Encapsulation of CDDP effectively inhibited tumor growth, while the encapsulation of BMP-2 promoted new bone formation.	In vitro study 4T-1, MG-63, SaOS-2, UMR-106 cells BMSCs study UMR-106 subcutaneous tumor in nude mice rabbit femoral defect model	127

**Table 3 (continued) | Scaffolds based on drug delivery system for osteosarcoma treatment and their role in bone regeneration**

Scaffold material	Therapeutic agents	Loading approach/Cross-Linking Method	Release time	Role in promotion bone regeneration	Study type	Study et al.
HEMA and MMA	DOX	electrostatic interaction	45 days	The scaffolds without DOX have been shown to induce osteodifferentiation of rBMCs	In vitro study rBMCs	136
PLLA/nHA	MET	Encapsulation/ Physical entrapment	49 days	MET-loaded scaffolds were found to promote osteogenic differentiation of hBMCs	In vitro study hBMCs and Saos-2 cells	134
PDA-coated LHAp and PLGA	DOX	Encapsulation of DOX-Loaded LHAp into the scaffold	20 days	PDA-coated scaffold showed enhanced bone growth after 20 days of drug release	In vitro study MG-63 and MC3T3-E1 cells study mice skull defect model	138

TCP tricalcium phosphate, HAp hydroxyapatite, DOX doxorubicin, CDDP cisplatin, PCL poly-ε-caprolactone, DXM dexamethasone, CS chitosan, nHA nanohydroxyapatite, ZoI zoledronic acid, GCT giant cell tumor of bone, hBMCs human bone marrow mesenchymal stem cells, CD cyclodextrin, pOBs primary osteoblasts, HUVECs human umbilical vein endothelial cells, PEEK polyetheretherketone, hFOB human fetal osteoblast cells, PLLA poly L-lactic acid, MTX methotrexate, CPC calcium phosphate cement, PLGA poly(lactide-co-glycolide), Sr strontium, NCTD Norcantharidin, HEMA/MMA hydroxyethyl methacrylate and methyl methacrylate, rBMCs bone marrow mesenchymal cells, MET metformin, PDA polydopamine, LHAp lamellar hydroxyapatite.

localized delivery of anti-tumor agents to combat malignancy. In a subcutaneous OS mouse model, MCSC/DOX scaffolds significantly suppressed tumor proliferation compared to MCSC alone. Additionally, MCSC scaffolds without DOX were evaluated in a critical-sized calvarial-defect rat model, revealing their capability to promote *in vivo* bone formation. In another study, Wang et al.<sup>147</sup> developed cryogenic 3D printed porous scaffolds incorporating 2D black phosphorus nanosheets, DOX, and osteogenic peptide, serving as the photothermal agent, anti-cancer medication, and osteogenic factor, respectively. Employing these scaffolds achieved tumor cell elimination and long-term prevention of tumor recurrence in a subcutaneous OS mouse model through on-demand photothermal therapy and sustained localized DOX release at a low concentration. *In vivo* outcomes indicated that photothermal therapy alone inadequately eliminates residual tumor cells, whereas sustained DOX release at low concentrations suppresses recurrence. In a separate cranial defect rat model, the scaffolds, initially irradiated by NIR laser for 10 min to mimic the anti-cancer stage, exhibited enhanced *in vivo* bone regeneration in cranial defects, attributable to the synergistic effects of the bony environment and sustained peptide release.

A preliminary study by Farzin et al.<sup>148</sup> explores combining magnetic fluid hyperthermia therapy with local drug delivery using a scaffold made of hardystonite loaded with Fe ions and CDDP. Further research is needed to understand how magnetically induced heating and drug delivery via these scaffolds affect cancer cell behavior and *in vivo* osteogenesis.

## Outlook

Osteosarcoma, the primary bone malignancy affecting children and young adults, poses significant challenges due to its malignancy, invasiveness, rapid progression, metastatic potential, and high mortality rate. The standard therapy, which involves surgery and chemotherapy, achieves long-term survival in over 60% of localized cases<sup>149</sup>. However, this approach is hindered by drawbacks such as toxicity, side effects, recurrence, drug resistance, and rapid blood clearance.

This review paper explores the potential of systemic NPs delivery for chemotherapy/therapeutic agents to enhance efficacy and minimize side effects. Despite exciting developments, challenges such as high clearance and accumulation in the liver, low tumor site accumulation, especially in bone tumors, and concerns about long-term biosafety, particularly for metal and ceramic NPs, remain inadequately assessed<sup>150,151</sup>.

Subsequently, we investigated the use of local-based drug delivery, with a specific focus on scaffold-based drug delivery. This approach serves a dual purpose: it effectively targets residual cancerous cells in the bone post-surgery through the localized administration of chemotherapeutic drugs, and it facilitates the eradication of any remaining tumor cells after surgery while minimizing potential side effects. Additionally, this system addresses the challenge of filling critical-sized bone defects resulting from the surgical removal of the bone tumor.

We then explored a new class of scaffolds, namely multifunctional scaffolds, which serve a third function beyond the dual purposes mentioned: they have been shown to induce bone regeneration. Despite advancements in recent studies on multifunctional scaffolds, limitations still exist. Firstly, studies that have developed scaffolds encapsulated with chemotherapeutic drugs have not examined the impact of the loaded therapeutic agent on healthy cells and osteogenesis<sup>136,138,146,147</sup>. The bone regeneration capacity of the scaffold has been tested without encapsulating the drugs or after releasing the chemotherapeutic drug, and then osteogenesis is assessed using *in vitro* or *in vivo*. This approach does not accurately represent the real bone tumor environment, where healthy cells are also affected by the high local concentration of chemotherapeutics. The toxicity of these drugs may hinder bone regeneration; thus, it is important to examine the effect of therapeutic agents on bone regeneration.

Secondly, the models used to examine the anticancer effectiveness of the scaffold often rely on ectopic tumor models, primarily at subcutaneous sites, which lack physiological and anatomical similarity to clinical conditions, thereby providing limited predictive value for clinical outcomes. Orthotopic

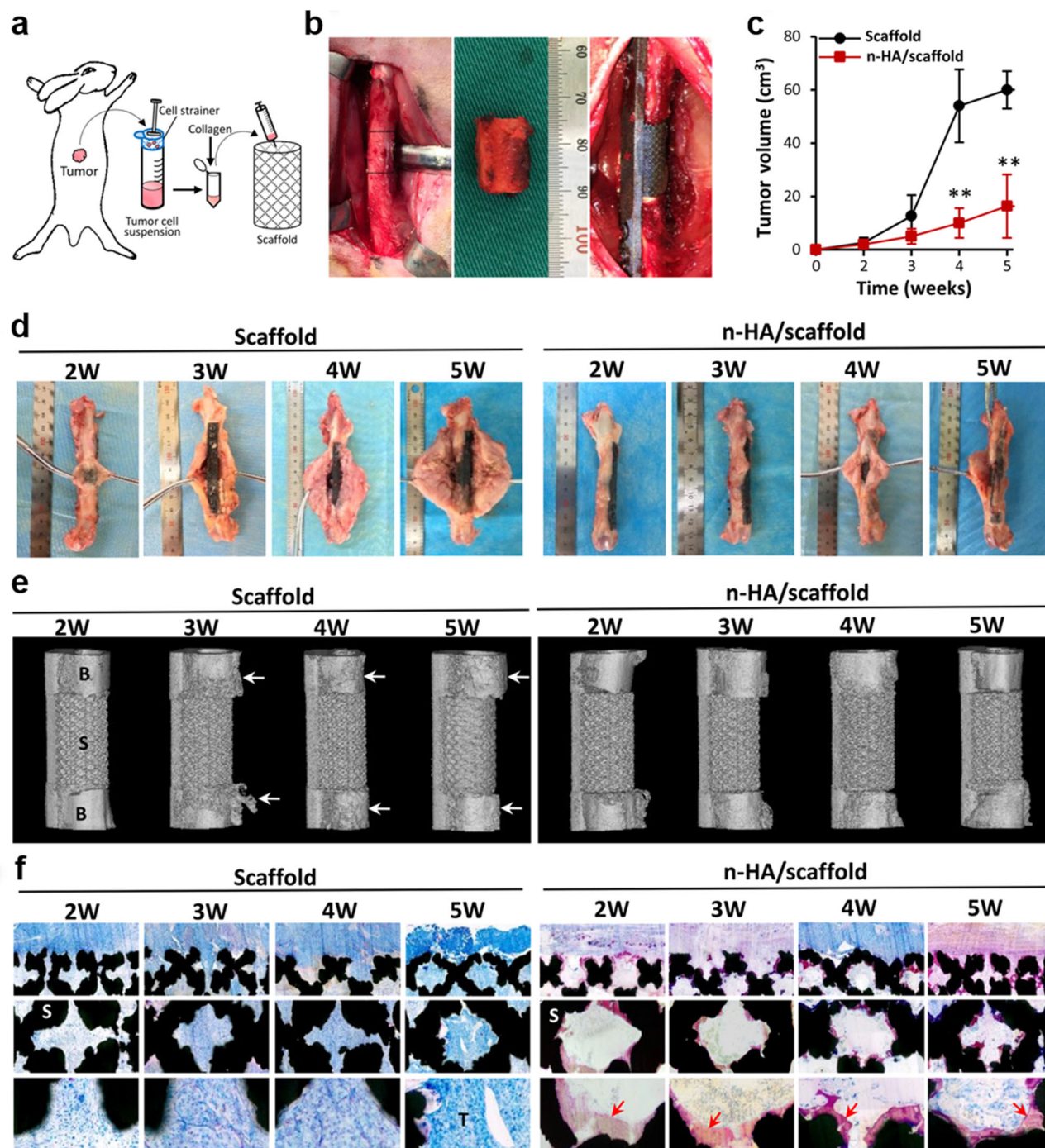


**Fig. 6 | Antitumor and segmental bone defect healing ability of n-HA-loaded titanium scaffold.** **a** Diagram depicting the preparation of tumor cell suspension and seeding into scaffold. **b** Implantation of tumor cell-seeded scaffold at segmental bone defect of rabbit femur. **c** Tumor volume of the rabbits implanted with empty scaffolds or n-HA/scaffolds within 5 weeks. Error bars represent SD.  $n = 4$  per group.  $**P < 0.01$  compared to empty scaffold, two-way  $t$  test. **d** Photographs of excised

implants with tumor from weeks 2 to 5. **e** Micro-CT-reconstructed images of the implants and adjacent bone tissue. B, bone; S, scaffold; arrows show adjacent cortical bone resorption by tumor. **f** Histological observation of the implanted scaffolds. S, scaffold; T, tumor; red arrows indicate new bone formation. (Adapted with permission from ref. 115).

models, which involve the implantation of tumor cell lines or patient-derived cell xenografts into the bone, provide a more reliable replication of the original tumor site. However, they present notable hurdles and technical complexities, particularly in mouse models, due to bone size constraints and challenges in scaffold insertion and tumor growth control<sup>152</sup>. A recent study has demonstrated the successful development of an orthotopic humanized tissue-engineered OS model in a genetically modified X-linked severe combined immunodeficient (X-SCID) rat<sup>153</sup>. Using an orthopedic OS model in rats

offers many advantages over mice, mainly because their larger size allows the development of larger tumors, which supports the conduction of clinically relevant diagnostic procedures such as medical imaging and properly executed biopsies. Additionally, the larger femur size in rats allows proper resection with appropriate margins, including a healthy tissue zone to ensure full tumor resection and subsequent filling with biomaterials.

Thirdly, identifying relevant preclinical animal models for the simultaneous examination of anti-tumor efficacy and bone regeneration remains

**Fig. 7 | Schematic illustration of MCSC scaffolds and their multi-functions.** The MCSC scaffolds exhibit excellent properties in drug delivery and simultaneously improve the efficacy of photothermal therapy under the irradiation of NIR laser. Additionally, the MCSC scaffolds also enhance new bone regeneration effectively by promoting osteogenic differentiation. NIR, near-infrared. (Reprinted with permission from ref. 147).

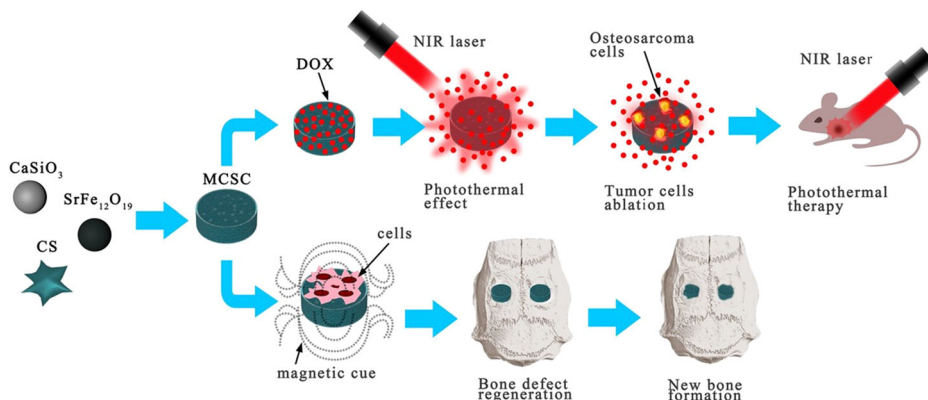


**Fig. 8 | Commonly employed animal models in the study of multifunctional scaffolds for anticancer therapy and bone tissue regeneration.** commonly used animal models in studies of multifunctional scaffolds are depicted. Typically, these studies examine anti-tumor efficacy and bone regeneration separately, with immunosuppressed rodent models preferred for bone malignancy and larger models, such as rabbits and rats, favored for bone regeneration. Created with BioRender.com.

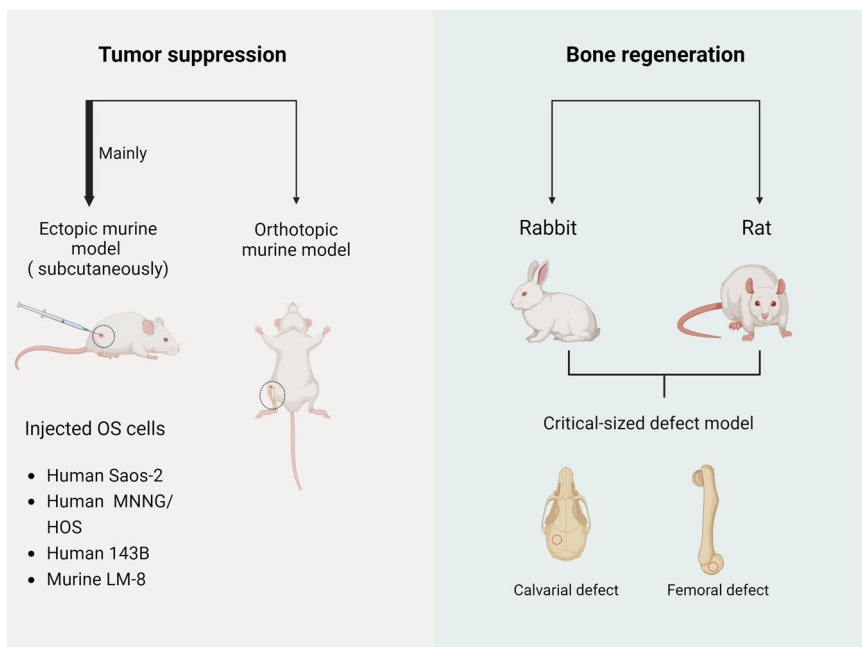


**Table 4 | Potential animal models for simultaneous assessment of tumor suppression and bone regeneration**

Model	Animal	OS cells	References
Segmental bone defect	New Zealand white rabbits	VX2 rabbit cells	115
Calvarial defect / Segmental bone defect	Fischer 344/NSIC rat	SOSN2 rat cells	146,161,162
Calvarial defect / Segmental bone defect	X-SCID rat	Humanized tissue-engineered bone niche	153
Calvarial defect	NUDE/SCID mice	Human OS cells such as MG-63 and Saos-2	163–165

SCID combined immune deficiency, OS osteosarcoma.

challenging. Typically, studies address these aspects separately, with immunosuppressed rodent models preferred for bone malignancy and larger models, such as rabbits and rats, favored for bone regeneration<sup>154,155</sup>, (Fig. 8). So far, only one study has reported testing the antitumor and bone regeneration ability of the scaffold simultaneously<sup>115</sup>. This was achieved by establishing a rabbit femur bone tumor model with VX2 tumor cells obtained from a tumor-bearing rabbit. While this model successfully demonstrated segmental bone defect repair after tumor resection, the use of human cell lines rather than rabbit cells remains crucial for ensuring translational relevance. Human cell lines offer a closer approximation to human disease, improving the reliability and applicability of research findings to human clinical settings.

To simultaneously evaluate scaffold functionality for bone defect repair and antitumor efficacy, two approaches are proposed:

1. Creating a bone defect and then implanting the scaffold with tumor cells into the defect site.
2. Transplanting OS cells into the bone via pretibial/intraosseous injection, followed by excising the developed tumor and implanting the scaffold.

A summary of potential animal models capable of assessing both anticancer efficacy and bone regeneration is presented in Table 4. Establishing more relevant models is crucial due to the variation in mineral density, mechanical cues, and biochemical composition of bones across

different species, including humans, sheep, mice, and rats. Therefore, success in animal models may not necessarily be directly translated to human patients. Consequently, bone substitutes that demonstrate efficacy in animal models may not necessarily be directly applicable to human patients, widening the gap between animal models and clinical application.

### Data availability

Data are available from the corresponding author upon reasonable request.

Received: 3 April 2024; Accepted: 13 August 2024;

Published online: 27 August 2024

### References

- van Oosterwijk, J. G., Anninga, J. K., Gelderblom, H., Cleton-Jansen, A. M. & Bovée, J. V. M. G. Update on targets and novel treatment options for high-grade osteosarcoma and chondrosarcoma. *Hematol. Oncol. Clin. North Am.* **27**, 1021–1048 (2013).
- Mirabello, L., Troisi, R. J. & Savage, S. A. Osteosarcoma incidence and survival rates from 1973 to 2004: data from the surveillance, epidemiology, and end results program. *Cancer* **115**, 1531–1543 (2009).
- Belayneh, R., Fourman, M. S., Bhogal, S. & Weiss, K. R. Update on osteosarcoma. *Curr. Oncol. Rep.* **23**, 1–8 (2021).
- Isakoff, M. S., Bielack, S. S., Meltzer, P. & Gorlick, R. Osteosarcoma: current treatment and a collaborative pathway to success. *J. Clin. Oncol.* **33**, 3029–3035 (2015).
- Tabone, M. D. et al. Osteosarcoma recurrences in pediatric patients previously treated with intensive chemotherapy. *J. Clin. Oncol.* **12**, 2614–2620 (1994).
- Yu, D. et al. Methotrexate, doxorubicin, and cisplatin regimen is still the preferred option for osteosarcoma chemotherapy. *Medicine* **98**, e15582 (2019).
- Sun, M. et al. A tissue-engineered therapeutic device inhibits tumor growth in vitro and in vivo. *Acta Biomater.* **18**, 21–29 (2015).
- Park, S. B. et al. Chemotherapy-induced peripheral neurotoxicity: a critical analysis. *CA Cancer J. Clin.* **63**, 419–437 (2013).
- Ma, H. et al. Localized co-delivery of doxorubicin, cisplatin, and methotrexate by thermosensitive hydrogels for enhanced osteosarcoma treatment. *ACS Appl Mater. Interfaces* **7**, 27040–27048 (2015).
- Haleem, A., Javaid, M., Singh, R. P., Rab, S. & Suman, R. Applications of nanotechnology in medical field: a brief review. *Glob. Health J.* **7**, 70–77 (2023).
- Zhang, Y. et al. Self-stabilized hyaluronate nanogel for intracellular codelivery of doxorubicin and cisplatin to osteosarcoma. *Adv. Sci.* **5**, 5 (2018).
- Li, K. et al. Calcium-mineralized polypeptide nanoparticle for intracellular drug delivery in osteosarcoma chemotherapy. *Bioact. Mater.* **5**, 721–731 (2020).
- Cai, J.-X. et al. Hybrid cell membrane-functionalized biomimetic nanoparticles for targeted therapy of osteosarcoma. *Int. J. Nanomed.* **17**, 837–854 (2022).
- González-Fernández Y., Brown H. K., Patiño-García A., Heymann D., and Blanco-Prieto M. J., Oral administration of edelfosine encapsulated lipid nanoparticles causes regression of lung metastases in pre-clinical models of osteosarcoma. *Cancer Lett.* **430**, <https://doi.org/10.1016/j.canlet.2018.05.030> (2018).
- Karlsson J., Vaughan H. J., and Green J. J., Biodegradable polymeric nanoparticles for therapeutic cancer treatments. *Annu. Rev. Chem. Biomol. Eng.* **9**, <https://doi.org/10.1146/annurev-chembioeng-060817-084055> (2018).
- Xiao X. et al. Polymeric nanoparticles — promising carriers for cancer therapy. *Front. Bioeng. Biotechnol.* **10**, <https://doi.org/10.3389/FBIOE.2022.1024143> (2022).
- Zielinska A. et al. Polymeric nanoparticles: production, characterization, toxicology and ecotoxicology. *Molecules* **25**, <https://doi.org/10.3390/MOLECULES25163731> (2020).
- Martella, E. et al. Functionalized Keratin as nanotechnology-based drug delivery system for the pharmacological treatment of osteosarcoma. *Int. J. Mol. Sci.* **19**, 3670 (2018).
- Li, S., Xiong, Y. & Zhang, X. Poloxamer surface modified trimethyl chitosan nanoparticles for the effective delivery of methotrexate in osteosarcoma. *Biomed. Pharmacother.* **90**, 872–879 (2017).
- de Castro K. C., Costa J. M., and Campos M. G. N., Drug-loaded polymeric nanoparticles: a review. *Int. J. Polym. Mater. Polym. Biomater.* **71**, <https://doi.org/10.1080/00914037.2020.1798436> (2022).
- Irmak G., Öztürk M. G., and Gümüşderelioğlu M., Salinomycin encapsulated PLGA nanoparticles eliminate osteosarcoma cells via inducing/inhibiting multiple signaling pathways: comparison with free salinomycin. *J. Drug Deliv. Sci. Technol.* **58**, <https://doi.org/10.1016/J.JDDST.2020.101834> (2020).
- Ni, M. Z. et al. Poly(lactic-co-glycolic acid) nanoparticles conjugated with CD133 aptamers for targeted salinomycin delivery to CD133+ osteosarcoma cancer stem cells. *Int. J. Nanomed.* **10**, 2537 (2015).
- Yin, X. et al. Chitooligosaccharides modified reduction-sensitive liposomes: enhanced cytoplasmic drug delivery and osteosarcomas-tumor inhibition in animal models. *Pharm. Res.* **34**, 2172–2184 (2017).
- Suk, J. S., Xu, Q., Kim, N., Hanes, J. & Ensign, L. M. PEGylation as a strategy for improving nanoparticle-based drug and gene delivery. *Adv. Drug Deliv. Rev.* **99**, 28 (2016).
- Ray, S., Saha, S., Sa, B. & Chakraborty, J. In vivo pharmacological evaluation and efficacy study of methotrexate-encapsulated polymer-coated layered double hydroxide nanoparticles for possible application in the treatment of osteosarcoma. *Drug Deliv. Transl. Res.* **7**, 259–275 (2017).
- Sharma, A., Goyal, A. K. & Rath, G. Recent advances in metal nanoparticles in cancer therapy. *J. Drug Target* **26**, 617–632 (2018).
- Yaqoob, A. A. et al. Recent advances in metal decorated nanomaterials and their various biological applications: a review. *Front. Chem.* **8**, 341 (2020).
- Sisubalan, N. et al. ROS-mediated cytotoxic activity of ZnO and CeO2 nanoparticles synthesized using the *Rubia cordifolia* L. leaf extract on MG-63 human osteosarcoma cell lines. *Environ. Sci. Pollut. Res. Int.* **25**, 10482–10492 (2018).
- Du, S. et al. Overendocytosis of superparamagnetic iron oxide particles increases apoptosis and triggers autophagic cell death in human osteosarcoma cell under a spinning magnetic field. *Oncotarget* **8**, 9410 (2017).
- He, G. et al. Cross talk between autophagy and apoptosis contributes to ZnO nanoparticle-induced human osteosarcoma cell death. *Adv. Healthc. Mater.* **7**, <https://doi.org/10.1002/ADHM.201800332> (2018).
- Seshadri, V. D. Zinc oxide nanoparticles from *Cassia auriculata* flowers showed the potent antimicrobial and in vitro anticancer activity against the osteosarcoma MG-63 cells. *Saudi J. Biol. Sci.* **28**, 4046–4054 (2021).
- Sun, J. et al. Progress of phototherapy applications in the treatment of bone cancer. *Int. J. Mol. Sci.* **22**, 11354 (2021).
- Xiong, S. et al. Gold nanoparticle-based nanoprobe with enhanced tumor targeting and photothermal/photodynamic response for therapy of osteosarcoma. *Nanotechnology* **32**, 155102 (2021).
- Popescu, R. C. et al. Fabrication and cytotoxicity of gemcitabine-functionalized magnetite nanoparticles. *Molecules* **22**, <https://doi.org/10.3390/MOLECULES22071080> (2017).
- Puiu, R. A. et al. Anti-cancer nanopowders and MAPLE-fabricated thin films based on SPIONs surface modified with paclitaxel loaded  $\beta$ -cyclodextrin. *Pharmaceutics* **13**, 1356 (2021).

36. Ghosh, S. et al. Development and physicochemical characterization of doxorubicin-encapsulated hydroxyapatite–polyvinyl alcohol nanocomposite for repair of osteosarcoma-affected bone tissues. *Comptes Rendus Chim.* **22**, 46–57 (2019).
37. Mabrouk, M., Moaness, M. & Beherei, H. H. Fabrication of mesoporous zirconia and titania nanomaterials for bone regeneration and drug delivery applications. *J. Drug Deliv. Sci. Technol.* **78**, 103957 (2022).
38. Cheng, Z. et al. Intracellular co-delivery of proteins and chemotherapeutics using calcium carbonate mineralized nanoparticles for osteosarcoma therapy. *Mater. Des.* **222**, <https://doi.org/10.1016/J.MATDES.2022.111040> (2022).
39. Mehnath, S., Karthikeyan, K., Rajan, M. & Jeyaraj, M. Fabrication of bone-targeting hyaluronic acid coupled alendronate-bioactive glass for osteosarcoma therapy. *Mater. Chem. Phys.* **273**, 125146 (2021).
40. Maia, A. L. C. et al. Vincristine-loaded hydroxyapatite nanoparticles as a potential delivery system for bone cancer therapy. *J. Drug Target* **26**, 592–603 (2018).
41. Zhou, Z. F. et al. Selenium-doped hydroxyapatite biopapers with an anti-bone tumor effect by inducing apoptosis. *Biomater. Sci.* **7**, 5044–5053 (2019).
42. Ghosh, S., Ghosh, S. & Pramanik, N. Bio-evaluation of doxorubicin (DOX)-incorporated hydroxyapatite (HAp)-chitosan (CS) nanocomposite triggered on osteosarcoma cells. *Adv. Compos Hybrid. Mater.* **3**, 303–314 (2020).
43. Ram Prasad, S., Jayakrishnan, A. & Sampath Kumar, T. S. Hydroxyapatite-dextran methacrylate core/shell hybrid nanocarriers for combinatorial drug therapy. *J. Mater. Res.* **35**, 2451–2465 (2020).
44. Liu, Y. et al. Bone mineral: a trojan horse for bone cancers. Efficient mitochondria targeted delivery and tumor eradication with nano hydroxyapatite containing doxorubicin. *Mater. Today Bio* **14**, 100227 (2022). **The use of doxorubicin-loaded nano/micro hydroxyapatite demonstrated a markedly greater reduction in tumor growth in an osteosarcoma mice model compared to the conventional systemic doxorubicin treatment regimen.**
45. Zhang, Y. et al. Tumor microenvironment-responsive hyaluronate-calcium carbonate hybrid nanoparticle enables effective chemotherapy for primary and advanced osteosarcomas. *Nano Res.* **11**, 4806–4822 (2018).
46. Zhao, P. et al. Selenium-doped calcium carbonate nanoparticles loaded with cisplatin enhance efficiency and reduce side effects. *Int. J. Pharm.* **570**, 118638 (2019). **Tumor microenvironment-responsive hyaluronate-calcium carbonate hybrid nanoparticles showed superior inhibition efficacy against both primary and advanced murine osteosarcoma models compared to free doxorubicin and non-crosslinked nanoparticles.**
47. Dan Son K. & Kim Y. J. Anticancer activity of drug-loaded calcium phosphate nanocomposites against human osteosarcoma. *Biomater. Res.* **21**, <https://doi.org/10.1186/S40824-017-0099-1> (2017).
48. Xiao, Y. et al. PEGylation and surface functionalization of liposomes containing drug nanocrystals for cell-targeted delivery. *Colloids Surf. B Biointerfaces* **182**, 110362 (2019).
49. Hama, S., Sakai, M., Itakura, S., Majima, E. & Kogure, K. Rapid modification of antibodies on the surface of liposomes composed of high-affinity protein A-conjugated phospholipid for selective drug delivery. *Biochem. Biophys. Rep.* **27**, 2405–5808 (2021).
50. Tefas, L. R. et al. Co-delivery of gemcitabine and salinomycin in PEGylated liposomes for enhanced anticancer efficacy against colorectal cancer. *J. Liposome Res.* **33**, 234–250 (2023).
51. Nunes, S. S. et al. Influence of PEG coating on the biodistribution and tumor accumulation of pH-sensitive liposomes. *Drug Deliv. Transl. Res.* **9**, 123–130 (2019).
52. Haghirsadat, F. et al. New liposomal doxorubicin nanoformulation for osteosarcoma: drug release kinetic study based on thermo and pH sensitivity. *Chem. Biol. Drug Des.* **90**, 368–379 (2017).
53. Haghirsadat, F. et al. A novel approach on drug delivery: investigation of a new nano-formulation of liposomal doxorubicin and biological evaluation of entrapped doxorubicin on various osteosarcoma cell lines. *Cell J.* **19**, 55–64 (2017).
54. Zhang, X. et al. HA-DOPE-modified Honokiol-loaded liposomes targeted therapy for osteosarcoma. *Int. J. Nanomed.* **17**, 5137–5151 (2022).
55. Zhao, L. et al. Polydopamine-based surface modification of paclitaxel nanoparticles for osteosarcoma targeted therapy. *Nanotechnology* **30**, 255101 (2019).
56. Niu, G. et al. Melatonin and doxorubicin co-delivered via a functionalized graphene-dendrimeric system enhances apoptosis of osteosarcoma cells. *Mater. Sci. Eng. C.* **119**, 111554 (2021).
57. Wu, V. M., Mickens, J. & Uskoković, V. Bisphosphonate-functionalized hydroxyapatite nanoparticles for the delivery of the bromodomain inhibitor JQ1 in the treatment of osteosarcoma. *ACS Appl. Mater. Interfaces* **9**, 25887–25904 (2017).
58. Lei, Z., Mengying, Z., Yifei, G., Xiangtao, W. & Meihua, H. Alendronate-modified polydopamine-coated paclitaxel nanoparticles for osteosarcoma-targeted therapy. *J. Drug Deliv. Sci. Technol.* **53**, 101133 (2019).
59. Wu, H., Luo, Y., Xu, D., Ke, X. & Ci, T. Low molecular weight heparin modified bone targeting liposomes for orthotopic osteosarcoma and breast cancer bone metastatic tumors. *Int. J. Biol. Macromol.* **164**, 2583–2597 (2020).
60. Zhou, X. et al. Bone-targeting polymer vesicles for simultaneous imaging and effective malignant bone tumor treatment. *Biomaterials* **269**, 120345 (2021).
61. Kang, N.-W., Lee, J.-Y. & Kim, D.-D. Hydroxyapatite-binding albumin nanoclusters for enhancing bone tumor chemotherapy. *J. Controll. Release* **342**, 111–121 (2022).
62. Chen, F. et al. Targeted salinomycin delivery with EGFR and CD133 aptamers based dual-ligand lipid-polymer nanoparticles to both osteosarcoma cells and cancer stem cells. *Nanomedicine* **14**, 2115–2127 (2018).
63. Gui, K. et al. Lipid-polymer nanoparticles with CD133 aptamers for targeted delivery of all-trans retinoic acid to osteosarcoma initiating cells. *Biomed. Pharmacother.* **111**, 751–764 (2019).
64. Yang, R. et al. The folate receptor  $\alpha$  is frequently overexpressed in osteosarcoma samples and plays a role in the uptake of the physiologic substrate 5-methyltetrahydrofolate. *Clin. Cancer Res.* **13**, 2557–2567 (2007).
65. Amiryaghoubi, N. et al. Smart chitosan–folate hybrid magnetic nanoparticles for targeted delivery of doxorubicin to osteosarcoma cells. *Colloids Surf. B Biointerfaces* **220**, 112911 (2022).
66. Karimian, A. et al. Synthesis of biocompatible nanocrystalline cellulose against folate receptors as a novel carrier for targeted delivery of doxorubicin. *Chem. Biol. Interact.* **351**, 109731 (2022).
67. Feng, S. et al. Engineering of bone- and CD44-dual-targeting redox-sensitive liposomes for the treatment of orthotopic osteosarcoma. *ACS Appl. Mater. Interfaces* **11**, 7357–7368 (2019).
68. Gazzano, E. et al. Hyaluronated liposomes containing H2S-releasing doxorubicin are effective against P-glycoprotein-positive/doxorubicin-resistant osteosarcoma cells and xenografts. *Cancer Lett.* **456**, 29–39 (2019). **Hyaluronated liposomes containing H2S-releasing doxorubicin overcome resistance.**
69. Chi, Y. et al. Redox-sensitive and hyaluronic acid functionalized liposomes for cytoplasmic drug delivery to osteosarcoma in animal models. *J. Controll. Release* **261**, 113–125 (2017).
70. Qiu, R., Sun, D., Bai, Y., Li, J. & Wang, L. Application of tumor-targeting peptide-decorated polypeptide nanoparticles with doxorubicin to treat osteosarcoma. *Drug Deliv.* **27**, 1704–1717 (2020).
71. Li, S. et al. Sarcoma-targeting peptide-decorated polypeptide nanogel intracellularly delivers shikonin for upregulated

- osteosarcoma necroptosis and diminished pulmonary metastasis. *Theranostics* **8**, 1361 (2018).
72. Haghirsadat, F. et al. Codelivery of doxorubicin and JIP1 siRNA with novel EphA2-targeted PEGylated cationic nanoliposomes to overcome osteosarcoma multidrug resistance. *Int. J. Nanomed.* **13**, 3853 (2018).
  73. Haghirsadat, F. et al. EphA2 targeted doxorubicin-nanoliposomes for osteosarcoma treatment. *Pharm. Res.* **34**, 2891–2900 (2017).
  74. Fang, Z. et al. Targeted osteosarcoma chemotherapy using RGD peptide-installed doxorubicin-loaded biodegradable polymeric micelle. *Biomed. Pharmacother.* **85**, 160–168 (2017).
  75. Drake, M. T., Clarke, B. L. & Khosla, S. Bisphosphonates: mechanism of action and role in clinical practice. *Mayo Clin. Proc.* **83**, 1032–1045 (2008).
  76. Jiao, J. et al. Redox and pH dual-responsive PEG and chitosan-conjugated hollow mesoporous silica for controlled drug release. *Mater. Sci. Eng. C.* **67**, 26–33 (2016).
  77. Fu, W. et al. In vitro evaluation of a novel pH sensitive drug delivery system based cockle shell-derived aragonite nanoparticles against osteosarcoma. *J. Exp. Nanosci.* **12**, 166–187 (2017).
  78. Sha, Z. et al. Manganese-doped gold core mesoporous silica particles as a nanoplatform for dual-modality imaging and chemodynamic combination osteosarcoma therapy. *Nanoscale* **13**, 5077–5093 (2021).
  79. Zhu, L. et al. Redox-responsive mesoporous silica nanoparticles for chemo- photodynamic combination cancer therapy. *Mater. Res. Express* **9**, 045401 (2022).
  80. Choi, Y. S. et al. Disrupting the redox balance with a diselenide drug delivery system: synergistic or antagonistic? *Adv. Funct. Mater.* **31**, <https://doi.org/10.1002/adfm.202007275> (2021).
  81. Fu, D. et al. A novel redox-responsive ursolic acid polymeric prodrug delivery system for osteosarcoma therapy. *Drug Deliv.* **28**, 195–205 (2021).
  82. Di Pompo, G., Cortini, M., Baldini, N. & Avnet, S. Acid microenvironment in bone sarcomas. *Cancers* **13**, 3848 (2021).
  83. Kato, Y. et al. Acidic extracellular microenvironment and cancer. *Cancer Cell Int.* **13**, 1 (2013).
  84. Zhu, Y. J. & Chen, F. pH-responsive drug-delivery systems. *Chem. Asian J.* **10**, 284–305 (2015).
  85. Wang, S.-Y., Hu, H.-Z., Qing, X.-C., Zhang, Z.-C. & Shao, Z.-W. Recent advances of drug delivery nanocarriers in osteosarcoma treatment. *J. Cancer* **11**, 69–82 (2020).
  86. Meshkini, A. & Oveisi, H. Methotrexate-F127 conjugated mesoporous zinc hydroxyapatite as an efficient drug delivery system for overcoming chemotherapy resistance in osteosarcoma cells. *Colloids Surf. B Biointerfaces* **158**, 319–330 (2017).
  87. Liu, J. et al. Hollow mesoporous silica nanoparticles facilitated drug delivery via cascade pH stimuli in tumor microenvironment for tumor therapy. *Biomaterials* **83**, 51–65 (2016).
  88. Yang, F., Wen, X., Ke, Q. F., Xie, X. T. & Guo, Y. P. pH-responsive mesoporous ZSM-5 zeolites/chitosan core-shell nanodisks loaded with doxorubicin against osteosarcoma. *Mater. Sci. Eng. C.* **85**, 142–153 (2018).
  89. Ahmadi, D. et al. Preparation and in-vitro evaluation of pH-responsive cationic cyclodextrin coated magnetic nanoparticles for delivery of methotrexate to the Saos-2 bone cancer cells. *J. Drug Deliv. Sci. Technol.* **57**, 101584 (2020).
  90. Zhang, X., Wang, S., Cheng, G., Yu, P. & Chang, J. Light-responsive nanomaterials for cancer therapy. *Engineering* **13**, 18–30 (2022).
  91. Martínez-Carmona, M., Lozano, D., Baeza, A., Colilla, M. & Vallet-Regí, M. A novel visible light responsive nanosystem for cancer treatment. *Nanoscale* **9**, 15967–15973 (2017).
  92. Chen, J. et al. Light-responsive micelles loaded with doxorubicin for osteosarcoma suppression. *Front. Pharm.* **12**, 1378 (2021).
  93. Lu, Y. et al. Enhancing osteosarcoma killing and CT imaging using ultrahigh drug loading and NIR-responsive Bismuth Sulfide@Mesoporous silica nanoparticles. *Adv. Health. Mater.* **7**, 19 (2018).
  94. Yang, P. et al. Doxorubicin and edelfosine combo-loaded lipid-polymer hybrid nanoparticles for synergistic anticancer effect against drug-resistant osteosarcoma. *Oncotargets Ther.* **13**, 8055–8067 (2020).
  95. Fumoto, S. & Nishida, K. Co-delivery systems of multiple drugs using nanotechnology for future cancer therapy. *Chem. Pharm. Bull.* **68**, 603–612 (2020).
  96. Caliskan, Y. et al. A new therapeutic combination for osteosarcoma: gemcitabine and clofazimine co-loaded liposomal formulation. *Int. J. Pharm.* **557**, 97–104 (2019). **The co-loaded liposomal formulation of Gemcitabine and Clofazimine exhibited higher cytotoxicity than their individual liposomal treatments.**
  97. He, C., Tang, Z., Tian, H. & Chen, X. Co-delivery of chemotherapeutics and proteins for synergistic therapy. *Adv. Drug Deliv. Rev.* **98**, 64–76 (2016).
  98. Hu, J. et al. Selenium-doped calcium phosphate biomineral reverses multidrug resistance to enhance bone tumor chemotherapy. *Nanomedicine* **32**, <https://doi.org/10.1016/j.nano.2020.102322> (2021).
  99. Stylianopoulos, T. & Jain, R. K. Design considerations for nanotherapeutics in oncology. *Nanomedicine* **11**, 1893–1907 (2015).
  100. Al Bostami, R. D., Abuwatfa, W. H. & Hussein, G. A. Recent advances in nanoparticle-based co-delivery systems for cancer therapy. *Nanomaterials* **12**, 2672 (2022).
  101. Wilhelm, S. et al. Analysis of nanoparticle delivery to tumours. *Nat. Rev. Mater.* **1**, 16014 (2016).
  102. Bae, Y. H. & Park, K. Targeted drug delivery to tumors: myths, reality and possibility. *J. Control. Release* **153**, 198–205 (2011).
  103. Giordano, F. et al. Nanodelivery systems face challenges and limitations in bone diseases management. *Adv. Ther.* **4**, <https://doi.org/10.1002/ADTP.202100152> (2021).
  104. Liu, Y. et al. Hydroxyapatite-bovine serum albumin-paclitaxel nanoparticles for locoregional treatment of osteosarcoma. *Adv. Health. Mater.* **10**, 2000573 (2021).
  105. Liu, Y. et al. Sustained and controlled delivery of doxorubicin from an in-situ setting biphasic hydroxyapatite carrier for local treatment of a highly proliferative human osteosarcoma. *Acta Biomater.* **131**, 555–571 (2021).
  106. Shoib, M., Saeed, A., Rahman, M. S. U. & Naseer, M. M. Mesoporous nano-bioglass designed for the release of imatinib and in vitro inhibitory effects on cancer cells. *Mater. Sci. Eng. C. Mater. Biol. Appl.* **77**, 725–730 (2017).
  107. Hoare, T. R. & Kohane, D. S. Hydrogels in drug delivery: progress and challenges. *Polym* **49**, 1993–2007 (2008).
  108. Saraf, S. et al. Poly(ethylene glycol)-poly(lactic-co-glycolic acid) based thermosensitive injectable hydrogels for biomedical applications. *J. Control Release* **172**, 715–729 (2013).
  109. Yang, Z. et al. The effect of PLGA-based hydrogel scaffold for improving the drug maximum-tolerated dose for in situ osteosarcoma treatment. *Colloids Surf. B Biointerfaces* **172**, 387–394 (2018). **The PLGA-based hydrogel for localized drug delivery yields better outcomes compared to the free drug administration.**
  110. Yang, Z., Liu, J. & Lu, Y. Doxorubicin and CD-CUR inclusion complex co-loaded in thermosensitive hydrogel PLGA-PEG-PLGA localized administration for osteosarcoma. *Int. J. Oncol.* **57**, 433–453 (2020).
  111. Si, M. et al. In situ co-delivery of doxorubicin and cisplatin by injectable thermosensitive hydrogels for enhanced osteosarcoma treatment. *Int. J. Nanomed.* **17**, 1309–1322 (2022).

112. Zheng, Y. et al. Injectable hydrogel-microsphere construct with sequential degradation for locally synergistic chemotherapy. *ACS Appl. Mater. Interfaces* **9**, 3487–3496 (2017).
113. Wang C., Ma Z., Yuan K., & Ji T. Using scaffolds as drug delivery systems to treat bone tumor. *Nanotechnology* **33**, <https://doi.org/10.1088/1361-6528/AC5017> (2022).
114. Maher, S., Kaur, G., Lima-Marques, L., Evdokiou, A. & Losic, D. Engineering of micro- to nanostructured 3D-printed drug-releasing titanium implants for enhanced osseointegration and localized delivery of anticancer drugs. *ACS Appl. Mater. Interfaces* **9**, 29562–29570 (2017).
115. Zhang, K. et al. Application of hydroxyapatite nanoparticles in tumor-associated bone segmental defect. *Sci. Adv.* **5**, <https://doi.org/10.1126/SCIADV.AAX6946> (2019). **The hydroxyapatite nanoparticles-releasing scaffold effectively suppressed tumor growth while simultaneously promoting bone regeneration in a critical-sized segmental bone defect in a rabbit tumor model.**
116. Ma, H., Feng, C., Chang, J. & Wu, C. 3D-printed bioceramic scaffolds: from bone tissue engineering to tumor therapy. *Acta Biomater.* **79**, 37–59 (2018).
117. Brunello, G. et al. The impact of bioceramic scaffolds on bone regeneration in preclinical in vivo studies: a systematic review. *Materials* **13**, 1500 (2020).
118. Bischoff, I. et al. In vitro evaluation of a biomaterial-based anticancer drug delivery system as an alternative to conventional post-surgery bone cancer treatment. *Mater. Sci. Eng. C.* **93**, 115–124 (2018). **Hypoxia protected primary endothelial cells and osteoblasts from the cytotoxic effects of doxorubicin.**
119. Bose, S., Sarkar, N. & Vahabzadeh, S. Sustained release of vitamin C from PCL coated TCP induces proliferation and differentiation of osteoblast cells and suppresses osteosarcoma cell growth. *Mater. Sci. Eng. C.* **105**, 110096 (2019).
120. Wu, Y. et al. 3D printed calcium phosphate cement (CPC) scaffolds for anti-cancer drug delivery. *Pharmaceutics* **12**, 1077 (2020).
121. Jones, E. et al. Natural polymeric scaffolds in bone regeneration. *Front. Bioeng. Biotechnol.* **1**, 474 [www.frontiersin.org](http://www.frontiersin.org) (2020).
122. Hartley, E., Moon, H. & Neves, A. Biodegradable synthetic polymers for tissue engineering: a mini-review. *Reinvent. Int. J. Undergraduate Res.* **15**, <https://doi.org/10.31273/REINVENTION.V15I1.801> (2022).
123. Wang, Y. et al. 3D printed biodegradable implants as an individualized drug delivery system for local chemotherapy of osteosarcoma. *Mater. Des.* **186**, 108336 (2020).
124. Sarkar, N. & Bose, S. Liposome-encapsulated curcumin-loaded 3D printed scaffold for bone tissue engineering. *ACS Appl. Mater. Interfaces* **11**, 17184–17192 (2019).
125. Ye, L. et al. 3D printed composite scaffolds incorporating ruthenium complex-loaded liposomes as a delivery system to prevent the proliferation of MG-63 cells. *Macromol. Mater. Eng.* **304**, 1900295 (2019).
126. Dewhurst, R. M. et al. Development of natural-based bone cement for a controlled doxorubicin-drug release. *Front. Bioeng. Biotechnol.* **8**, 754 (2020).
127. Jiang, Y. et al. Bioinspired adhesive and tumor microenvironment responsive nanoMOFs assembled 3D-printed scaffold for anti-tumor therapy and bone regeneration. *Nano Today* **39**, 101182 (2021).
128. Roohani-Esfahani, S. I. et al. Unique microstructural design of ceramic scaffolds for bone regeneration under load. *Acta Biomater.* **9**, <https://doi.org/10.1016/j.actbio.2013.02.039> (2013).
129. Mirkhalaf, M. et al. Highly substituted calcium silicates 3D printed with complex architectures to produce stiff, strong and bioactive scaffolds for bone regeneration, *Appl. Mater Today* **25**, <https://doi.org/10.1016/j.apmt.2021.101230> (2021).
130. Entezari, A. et al. Unraveling the influence of channel size and shape in 3D printed ceramic scaffolds on osteogenesis. *Acta Biomater.* **180**, 115–127 (2024).
131. Hutmacher, D. W. Scaffolds in tissue engineering bone and cartilage. *Biomaterials* **21**, 2529–2543 (2000).
132. Ikada, Y. Challenges in tissue engineering. *J. R. Soc. Interface* **3**, 589–601 (2006).
133. Albrektsson, T. & Johansson, C. Osteoinduction, osteoconduction and osseointegration. *Eur. Spine J.* **10**, S96–S101 (2001).
134. Tan, W. et al. Dual-functional scaffolds of poly(L-lactic acid)/nanohydroxyapatite encapsulated with metformin: Simultaneous enhancement of bone repair and bone tumor inhibition. *Mater. Sci. Eng. C.* **120**, 111592 (2021). **The poly (L-lactic acid)/nanohydroxyapatite encapsulated with metformin scaffold can simultaneously enhance bone repair and inhibit bone tumor formation in vitro.**
135. Lu, Y. et al. High-activity chitosan/nano hydroxyapatite/zoledronic acid scaffolds for simultaneous tumor inhibition, bone repair and infection eradication. *Mater. Sci. Eng. C.* **82**, 225–233 (2018).
136. Sreeja, S., Parameshwar, R., Varma, P. R. H. & Sailaja, G. S. Hierarchically porous osteoinductive poly(hydroxyethyl methacrylate-co-methyl methacrylate) scaffold with sustained doxorubicin delivery for consolidated osteosarcoma treatment and bone defect repair. *ACS Biomater. Sci. Eng.* **7**, 701–717 (2021).
137. Huang, Z. et al. Strontium/Chitosan/Hydroxyapatite/Norcantharidin composite that inhibits osteosarcoma and promotes osteogenesis in vitro. *Biomed. Res. Int.* **2020**, <https://doi.org/10.1155/2020/9825073> (2020).
138. Lu, Y. et al. Enwrapping polydopamine on doxorubicin-loaded lamellar hydroxyapatite/poly(lactic-co-glycolic acid) composite fibers for inhibiting bone tumor recurrence and enhancing bone. *Regenerat. ACS Appl. Bio. Mater.* **4**, 6036–6045 (2021).
139. Ma, L. et al. A novel photothermally controlled multifunctional scaffold for clinical treatment of osteosarcoma and tissue regeneration. *Mater. Today* **36**, 48–62 (2020).
140. Dong, S., Chen, Y., Yu, L., Lin, K. & Wang, X. Magnetic hyperthermia-synergistic H<sub>2</sub>O<sub>2</sub> self-sufficient catalytic suppression of osteosarcoma with enhanced bone-regeneration bioactivity by 3D-printing composite scaffolds. *Adv. Funct. Mater.* **30**, 1907071 (2020).
141. Liao, J., Shi, K., Jia, Y., Wu, Y. & Qian, Z. Gold nanorods and nanohydroxyapatite hybrid hydrogel for preventing bone tumor recurrence via postoperative photothermal therapy and bone regeneration promotion. *Bioact. Mater.* **6**, <https://doi.org/10.1016/j.bioactmat.2021.01.006> (2021).
142. Dang, W. et al. A bifunctional scaffold with CuFeSe<sub>2</sub> nanocrystals for tumor therapy and bone reconstruction. *Biomaterials* **160**, 92–106 (2018).
143. Bigham, A., Aghajanian, A. H., Allahdaneh, S. & Hassanzadeh-Tabrizi, S. A. Multifunctional mesoporous magnetic Mg<sub>2</sub>SiO<sub>4</sub>-CuFe<sub>2</sub>O<sub>4</sub> core-shell nanocomposite for simultaneous bone cancer therapy and regeneration. *Ceram. Int.* **45**, 19481–19488 (2019).
144. Ansari, M., Bigham, A. & Ahangar, H. A. Super-paramagnetic nanostructured CuZnMg mixed spinel ferrite for bone tissue regeneration. *Mater. Sci. Eng. C.* **105**, 110084 (2019).
145. Iqbal, Y., Bae, H., Rhee, I. & Hong, S. Control of the saturation temperature in magnetic heating by using polyethylene-glycol-coated rod-shaped nickel-ferrite (NiFe<sub>2</sub>O<sub>4</sub>) nanoparticles. *J. Korean Phys. Soc.* **68**, 587–592 (2016).
146. Yang, F. et al. Magnetic mesoporous calcium silicate/chitosan porous scaffolds for enhanced bone regeneration and photothermal-chemotherapy of osteosarcoma. *Sci. Rep.* **8**, 7345 (2018).
147. Wang, C. et al. Cryogenic 3D printing of porous scaffolds for in situ delivery of 2D black phosphorus nanosheets, doxorubicin hydrochloride and osteogenic peptide for treating tumor resection-induced bone defects. *Biofabrication* **12**, <https://doi.org/10.1088/1758-5090/AB6D35> (2020).

148. Farzin, A., Fathi, M. & Emadi, R. Multifunctional magnetic nanostructured hardyostone scaffold for hyperthermia, drug delivery and tissue engineering applications. *Mater. Sci. Eng. C*. **70**, 21–31 (2017).
149. Gill, J. & Gorlick, R. Advancing therapy for osteosarcoma. *Nat. Rev. Clin. Oncol.* **18**, 609–624 (2021).
150. Sun, L., Sogo, Y., Wang, X. & Ito, A. Biosafety of mesoporous silica nanoparticles: a combined experimental and literature study. *J. Mater. Sci. Mater. Med.* **32**, 102 (2021).
151. Su, H. et al. Potential applications and human biosafety of nanomaterials used in nanomedicine. *HHS Public Access J. Appl. Toxicol.* **38**, 3–24 (2018).
152. Yang, Q. et al. Engineering 2D mesoporous Silica@MXene-integrated 3D-printing scaffolds for combinatory osteosarcoma therapy and NO-augmented bone regeneration. *Small* **16**, 1906814 (2020).
153. Lahr, C. A. et al. A humanised rat model of osteosarcoma reveals ultrastructural differences between bone and mineralised tumour tissue. *Bone* **158**, <https://doi.org/10.1016/j.bone.2021.116018> (2022). **Orthotopic humanized osteosarcoma rat model replicates pathognomonic features of human osteosarcoma.**
154. Guijarro, M. V., Ghivizzani, S. C. & Gibbs, C. P. Animal models in osteosarcoma. *Front. Oncol.* **4**, 103633 (2014).
155. McGovern, J. A., Griffin, M. & Huttmacher, D. W. Animal models for bone tissue engineering and modelling disease. *Dis. Model Mech.* **11**, 4 (2018).
156. Xi, Y. et al. Dual targeting curcumin loaded alendronate-hyaluronan-octadecanoic acid micelles for improving osteosarcoma therapy. *Int. J. Nanomed.* **14**, 6425–6437 (2019).
157. Li, Y., Qu, J., Zhang, P. & Zhang, Z. Reduction-responsive sulfur dioxide polymer prodrug nanoparticles loaded with irinotecan for combination osteosarcoma therapy. *Nanotechnology* **31**, 455101 (2020).
158. Zheng, Y. et al. A new type of glutathione-responsive anti-osteosarcoma prodrug nanoparticles. *Mater. Technol.* **37**, 953–961 (2022).
159. Hess, U. et al. Co-delivery of cisplatin and doxorubicin from calcium phosphate beads/matrix scaffolds for osteosarcoma therapy. *Mater. Sci. Eng. C*. **77**, 427–435 (2017).
160. Ouyang, L. et al. Smart release of doxorubicin loaded on polyetheretherketone (PEEK) surface with 3D porous structure. *Colloids Surf. B Biointerfaces* **163**, 175–183 (2018).
161. Tanzawa Y. et al. Potentiation of the antitumor effect of calcium phosphate cement containing anticancer drug and caffeine on rat osteosarcoma. *J. Orthop. Sci.* **16**, <https://doi.org/10.1007/s00776-011-0045-3> (2011).
162. Spicer, P. P. et al. Evaluation of bone regeneration using the rat critical size calvarial defect. *Nat. Protoc.* **7**, <https://doi.org/10.1038/nprot.2012.113> (2012).
163. Guo, T., Yuan, X., Li, X., Liu, Y. & Zhou, J. Bone regeneration of mouse critical-sized calvarial defects with human mesenchymal stem cell sheets co-expressing BMP2 and VEGF. *J. Dent. Sci.* **18**, <https://doi.org/10.1016/j.jds.2022.06.020> (2023).
164. Samsonraj, R. M. et al. A versatile protocol for studying calvarial bone defect healing in a mouse model. *Tissue Eng. Part C Methods* **23**, <https://doi.org/10.1089/ten.tec.2017.0205> (2017).
165. Uluçkan Ö., Segaliny A., Botter S., Santiago J. M. & Mutsaers A. J. Preclinical mouse models of osteosarcoma. *Bonekey Rep.* **4**, <https://doi.org/10.1038/bonekey.2015.37> (2015).

## Acknowledgements

The authors acknowledge the Australian Research Council for Industrial Transformation Training Centres (Grant No. IC170100022).

## Author contributions

S.K. initiated this manuscript. S.K. contributed to the research and discussion of all topics. S.K. wrote the manuscript with contributions from Z.L. and H.Z. H.Z. raised the funding that supported this study. All authors discussed and revised the manuscript and have given approval for its final version.

## Competing interests

The authors declare no competing interests.

## Additional information

**Supplementary information** The online version contains supplementary material available at <https://doi.org/10.1038/s43246-024-00612-2>.

**Correspondence** and requests for materials should be addressed to Hala Zreiqat.

**Peer review information** *Communications Materials* thanks Quinn Besford, Gagan Jalandhra and the other, anonymous, reviewer(s) for their contribution to the peer review of this work. Primary Handling Editors: Daniela Loessner and John Plummer. A peer review file is available.

**Reprints and permissions information** is available at <http://www.nature.com/reprints>

**Publisher's note** Springer Nature remains neutral with regard to jurisdictional claims in published maps and institutional affiliations.

**Open Access** This article is licensed under a Creative Commons Attribution-NonCommercial-NoDerivatives 4.0 International License, which permits any non-commercial use, sharing, distribution and reproduction in any medium or format, as long as you give appropriate credit to the original author(s) and the source, provide a link to the Creative Commons licence, and indicate if you modified the licensed material. You do not have permission under this licence to share adapted material derived from this article or parts of it. The images or other third party material in this article are included in the article's Creative Commons licence, unless indicated otherwise in a credit line to the material. If material is not included in the article's Creative Commons licence and your intended use is not permitted by statutory regulation or exceeds the permitted use, you will need to obtain permission directly from the copyright holder. To view a copy of this licence, visit <http://creativecommons.org/licenses/by-nc-nd/4.0/>.

© The Author(s) 2024